Software Interface Specification for the Hayabusa2 LIDAR Data Products

Version 1.2.1

February 3, 2025

Prepared by
Koji Matsumoto[1], Hirotomo Noda[1], Hiroki Senshu[2], Shin-ya Murakami[3], Ryuhei Yamada[4], Shoko Oshigami[3], Keiko Yamamoto[1], Hiroshi Araki[1]

1: RISE Project, National Astronomical Observatory of Japan
2: Planetary Exploration Research Center, Chiba Institute of Technology
3: Japan Aerospace Exploration Agency
4: The University of Aizu

Table of Contents

Change Log

DATE	CHANGE	AFFECTED SECTIONS
2015-10-02	Initial draft template	
2017-10-24	First draft	All
2017-12-25	Second draft	All
2020-04-10	Third draft	All
2020-05-29	Fourth draft	6.2
2020-06-14	Fifth draft	2, 5 and 6
2020-06-18	Sixth draft	6.2
2020-07-16	Seventh draft	5.1, 5.3, 6.2
2021-06-25	Eighth draft	5 and 6
2022-01-05	Ninth draft	All
2022-10-05	Version 1.0	All
2024-10-01	Version 1.1.9 - Added/Updated description on LIDAR Derived Time Series Albedo Data and LIDAR Derived Albedo Map products - Applied editorial changes to all sections	2, 5.2, 5.3.2.2.4, 5.3.2.3.4, 5.3.2.3.5, 5.3.3, 6.1, 6.2.13, 6.2.14
2024-10-02	Version 1.2.0 - Fixed error of Equation (24): M/10 is replaced with 10/M	5.3.2.3.4
2025-02-03	Version 1.2.1 - Corrected description of LIDAR Derived Albedo Map product - Updated generation proceduce of the LIDAR Derived Time Series Albedo Data product	5.2, 5.3.2.3.4, 5.3.2.3.5, 6.2.1 Table 23

Acronyms and Abbreviations

Acronym/Abbreviation	Definition
AOCS	Attitude and Orbit Control System
AOCSM	packet type which is related to AOCS for mission instruments
AOCU	Attitude and Orbit Control Unit
APD	Avalanche Photodiode
ASCII	American Standard Code for Information Interchange
C-SODA	Center for Science satellite Operation and Data Archive
CK	Orientation or Attitude kernel (“C-Matrix” kernel)
CODMAC	Committee On Data Management And Computation
DAC	Data Archive Team
DC/DC	DC (Direct Current) to DC converter
DHU	Data Handling Unit
DN	Digital Number
DSV	Delimiter-Separated Values
DU	Digital Unit
ESTM	Estimated ephemeris
ET	Ephemeris Time; Ephemeris seconds past J2000
FK	Frames kernel
FOV	Field Of View
HIC	Hybrid Integrated Circuit
HK	House Keeping
HPK	Home Position Keeping
IAU	International Astronomical Union
IK	Instrument kernel
IPDA	International Planetary Data Alliance
ISAS	Institute of Space and Astronautical Science
JATOPS	JAXA Approach Trajectory Optimizer with Statistic constraints
JAXA	Japan Aerospace Exploration Agency
LIDAR	Light Detection And Ranging
LSB	Least Significant Bit
LSK	Leapseconds kernel
MCMC	Markov chain Monte Carlo
NAVSENS	packet type which is related to navigation by remote sensing
OP-NAV	trajectory created from optical navigation
PCK	Planetary Constants kernel
PDS	Planetary Data System
PI	Principal Investigator
PFM	Proto Flight Model
SBN	Small Bodies Node

Acronym/Abbreviation	Definition
SCLK	Spacecraft Clock kernel
SIS	Software Interface Specification
SPC	Stereophotoclinometry
SPK	Ephemeris data kernel
SPICE	Spacecraft, Planet, Instruments, C-Matrix, Events
SIRIUS	Scientific Information Retrieval and Integrated Utilization System
SLR	Satellite Laser Ranging
TI	Time Indicator
TOF	Time Of Flight
UTC	Coordinated Universal Time
XML	Extensible Markup Language
YAG	Yttrium Aluminum Garnet

1 Purpose and Scope of Document

The purpose of this Data Product Software Interface Specification (SIS) is to provide users of the raw, calibrated, and derived data products from the Hayabusa2 LIDAR with a detailed description of the products, and a description of how the products were generated, including sources and destinations. The products defined in this document are time-series range data, topographic data, laser link experiment data, dust count data, albedo information, and spacecraft trajectory derived from time-series range data.

The SIS is intended to provide enough information to enable users to read and understand the LIDAR data products as stored in the PDS. The users for whom this SIS is intended are software developers of the programs used in generating the LIDAR products and scientists who will analyze the data, including those associated with the Hayabusa2 mission, LIDAR instrument and those in the general planetary science community.

2 Applicable Documents

This SIS is consistent with the following Planetary Data System Documents as adopted by the International Planetary Data Alliance (IPDA):

1. Planetary Data System Standards Reference, Version 1.14.0, May 22, 2020.
2. PDS4 Data Dictionary – Abridged – Version 1.14.0.0, March 23, 2020.
3. PDS4 Information Model Specification, Version 1.14.0.0, March 23, 2020.

This SIS is responsive to the following Hayabusa2 mission document(s):

4. Science Policy for Hayabusa2 Project, Version 3.0, May 14, 2018.

This SIS makes reference to the following documents:

5. Mizuno et al., Development of the Laser Altimeter (LIDAR) form Hayabusa2, *Space Science Reviews,* **208**:33-47*,* https://doi.org/10.1007/s11214-015-0231-2, 2017.
6. Senshu et al., Dust Detection Mode of the Hayabusa2 LIDAR, *Space Science Reviews*, **208**:65-79, https://doi.org/10.1007/s11214-016-0242-7, 2017.
7. Noda et al., Laser link experiment with the Hayabusa2 laser altimeter for in-flight alignment measurement, *Earth, Planets and Space*, **69**:2, https://doi.org/10.1186/s40623-016-0589-8, 2017.
8. Yamada et al., Albedo Observation by Hayabusa2 LIDAR: Instrument Performance and Error Evaluation, *Space Science Reviews*, **208**:49-64, https://doi.org/10.1007/s11214-016-0240-9, 2017.
9. Matsumoto et al., Improving Hayabusa2 trajectory by combining LIDAR data and a shape model, *Icarus*, **338**, 113574, https://doi.org/10.1016/j.icarus.2019.113574, 2020.
10. Yamamoto et al., Dynamic precise orbit determination of Hayabusa2 using laser altimeter (LIDAR) and image tracking data sets, *Earth, Planets and Space*, **72**:85, https://doi.org/10.1186/s40623-020-01213-2, 2020.
11. Yamada et al., Derivation of 1.064 μm normal albedos on the C-type asteroid Ryugu from laser pulse intensity measurement of the Hayabusa2 LIDAR, *Earth, Planets and Space*, **74**:166, https://doi.org/10.1186/s40623-022-01717-z, 2022.
12. Yamada et al., Correction: Derivation of 1.064 μm normal albedos on the C-type asteroid Ryugu from laser pulse intensity measurement of the Hayabusa2 LIDAR, *Earth, Planets and Space*, **76**:17, https://doi.org/10.1186/s40623-023-01949-7, 2024.

3 Configuration Management

The Hayabusa2 LIDAR team controls the data products described in this document, as well as the document itself. Requests for changes to the data products, or the scope and contents of the document are made to the Science PI of the Hayabusa2 LIDAR team, Noriyuki Namiki. An engineering change request will be evaluated against its impact on the LIDAR ground data processing system before acceptance. Once a change request has been approved, software and documentation are updated, version numbers incremented, tested, and finally released for production.

The data products and documentation described in this SIS as well as the SIS itself have completed a formal PDS peer review and lien resolution process. The peer review ensures that all data products described by this SIS comply with PDS4 standards as noted in Section 2 – Applicable Documents. The PDS peer review panel consisted of members of the PDS Small Bodies Node (SBN) and members of the planetary science community. Any changes to data products subsequent to the peer review, will be reviewed internally by the PDS SBN to determine if an additional peer review is necessary.

4 Relationships with Other Interfaces

Changes to the data products described in this SIS affect the software, products, or document in Table 1.

Table 1. Interface relationships

Name of Interface	Type	Owner
LIDAR Database Schema	Product	LIDAR Team
LIDAR Raw Science Data	Product	LIDAR Team
LIDAR Raw Housekeeping Data	Product	LIDAR Team
Science Policy for Hayabusa2	Document	Project
LIDAR Ground Data Processing	Software	LIDAR Team
LIDAR Archive Software	Software	LIDAR Team, DAC Team

A systems engineering approach is used to evaluate how changes in any one of these interfaces affects the others. It is possible that changes to one of these items will not affect any other item.

5 Data Product Characteristics and Environment

5.1 Instrument Overview

The Hayabusa2 LIDAR (Light Detection And Ranging) laser altimeter instrument measures the distance from the spacecraft to a target. The LIDAR has two primary functions for the Hayabusa2 mission, first as a navigation sensor to aid in asteroid rendezvous, approach, and touchdown procedures; and second as a scientific instrument to study the topography, gravity and surface reflectivity (albedo) of asteroid (162173) Ryugu. LIDAR measures not only ranges but also the intensity of transmitted and received laser pulses. LIDAR is an active sensor, unlike other instruments aboard Hayabusa2, and the ratio of transmitted and received energy can be translated into normal albedo on the surface of Ryugu (Mizuno et al., 2017).

The LIDAR system is a pulse radar that uses a YAG laser (fundamental wavelength: 1064 nm) as a transmitting light source, and it measures distances by measuring the time-of-flight (TOF) of the laser pulse. The LIDAR is installed on the -Z panel of Hayabusa2 spacecraft, with the aperture of optics (transmission and receptions) directed approximately in the -Z direction.

LIDAR emits laser light and measures the time duration between transmission and reception with time resolution of 3.33 ns, which corresponds to the spatial resolution of 0.5 m. The wavelength of laser light is 1064 nm (YAG-laser), and emitted from a passive Q switched Nd:YAG at a maximum rate of 1 Hz. The pulse width of laser light is 7 ns, and the total energy of each shot is 15 mJ. The beam divergence angle of the laser is 2.4 mrad. The LIDAR measures the energies of transmission and reception, simultaneously. The returned pulse is detected when the energy flux exceeds a threshold value. The measured amount of energy is recorded as 8-bit resolution telemetry.

To meet all operational and observation requirements, the LIDAR on Hayabusa2 must operate over a distance of 25 km to 30 m from Ryugu. The dynamic range requirement is met by two types of receiver optics. One is for "FAR" range and another is for "NEAR" range. The received light level of the FAR optics is 1345 times that of the NEAR optics, allowing the LIDAR to perform measurements over a wide dynamic range. The field of view (FOV) of FAR and NEAR optics are 1.5 mrad and 20.4 mrad, respectively. The gain or multiplication factor (denoted by M) of reception optics element (avalanche photodiode, APD) is chosen from high ($M = 100$), middle ($M = 33$), low ($M = 10$), and very low ($M = 0.1$) for both of FAR and NEAR optics, respectively. Table 2 provides a quick reference for all LIDAR specifications. The number of LIDAR shots during proximity phase was about seven million.

Table 2. LIDAR specifications from Mizuno et al. (2017)

Characteristic	Specification
Range	30 m–25 km (expected albedo: 0.06–0.1)
Resolution	0.5 m
Accuracy (1σ)	±1 m (at 30 m) < ±5.5 m (at 25 km)
Repetition Rate	Driven by an external trigger. Max. 1 Hz
Laser transmitter	Monolithic passive Q-SW Nd:YAG + Cr Wavelength: 1064 nm; Pulse energy: 15 mJ; Pulse width: 7 ns
Receiver optics	Long range (>1 km): effective diameter: 110 mm (Cassegrain, SiC), FOV: 1.5 mrad Short range (<1 km): effective diameter: 3 mm, FOV: 20.4 mrad
Receiver detector	Si APD-HIC
Telemetry data	17-bit range data (equivalent to range from 0 km to 65 km) Monitors for the transmitting laser energy and received signal energy Hardware statuses Total size of one telemetry data is 10 words (1 word = 16 bits).
Electrical interfaces	Voltage: +30.5–51 V Power consumption: 18 W Communication: RS-422
Mechanical Interfaces	Dimensions: 241 × 228 × 229 mm Weight: 3.52 kg (including DC/DC, radiator)
Thermal interfaces	Storage temperature: −30 to +60 °C Operating temperature: +10 to +40 °C

In addition to normal ranging mode, the LIDAR on board Hayabusa2 has two other operational modes: laser link mode and dust count mode.

5.1.1 Laser Link Mode

The Hayabusa2 LIDAR has a transponder function that allows the LIDAR to be used as a transponder. The LIDAR transponder function transmits a laser pulse immediately after receiving a

laser pulse. This is called the “triggered response transponder” function. The time from reception to transmission is measured and sent to the ground as telemetry data. Noda et al. (2017) describes a laser ranging experiment conducted between Hayabusa2 and an Earth-based ground station used for satellite laser ranging (SLR) in the winter of 2015. Another experiment was conducted in 2020 for which data are not included in this archive.

The LIDAR has a transponder function to return responder pulses, responding to a laser pulse from a ground station as an interrogator. In transponder mode, the LIDAR opens the receiving gate and waits for a laser pulse. If a laser from the ground station is received, the LIDAR will transmit the laser immediately. This receiving time and the laser transmitting time are sent by the usual communications link as telemetry data. The TOF is measured using a highly precise ground-based clock system. Therefore, the “triggered response transponder” function for SLR can be implemented using a simple clock system on the spacecraft. The LIDAR can respond to both single and double pulses from the ground station. When a double pulse is used, we can calibrate the LIDAR counter by measuring the double pulse interval at both the LIDAR and the ground station. The LIDAR transmits a single pulse even when a double pulse is received.

LIDAR data products produced from the Earth Swing-by observation campaign in 2015 are all Laser Link Mode data products, except for one short data period in ranging mode to monitor the laser signal intensity.

5.1.2 Dust Count Mode

We take advantage of the wide dynamic range of the Hayabusa2 LIDAR to detect dust possibly lofting above the asteroid’s surface. A new function called “dust count” is implemented on the Hayabusa2 LIDAR to observe the spatial distribution of dust density with a resolution of 20 m along the line-of-sight direction.

In terrestrial atmospheric observations, LIDAR is used to measure the distribution of aerosol grains along the line of sight from the profile of the return pulse. On the contrary, in the case of Hayabusa2, the energy profile is too large to be downlinked to Earth, because the link budget between the spacecraft and the ground station is quite limited. To reduce the data size, we applied the following measures: (1) the dust count range is limited to a part of the line of sight, (2) this dust count range is divided into 50 bins, and (3) the power of the signal in each bin is compared with a certain threshold. The size of the observation data is only 50 bits for each shot. On the basis of the scientific requirement that the temporal resolution of the dust count be as high as possible, we set the duration of each bin to a constant value of 133.33 ns, corresponding to a spatial resolution of 20 m, resulting in a total observation range of 1 km. The distance to the initial point of the dust count range is variable and can be set between 0 and 127 μs in increments of 1 μs. This corresponds to a change of the initial point d_1 from the vicinity of the spacecraft to a distance of 19.05 km from the spacecraft in units of 0.15 km. We can therefore search for signs of dust around the target asteroid even from an altitude of 20 km. However, it should be noted that the farther the dust count range is set, the fainter the signal from the dust grains becomes because of geometric attenuation. Therefore, dust observations were made not only at high altitude (Box-A) but also at low altitude (Box-C). A full description of the dust detection mode can be found in Senshu et al. (2017), from which most of the preceding paragraph was taken.

5.2 Data Product Overview

The LIDAR data products are time series data and map-type data. The time series data are created for laser link experiment, LIDAR range, topographic height, dust count, and albedo. The map-type data product is global grid data of albedo.

The LIDAR data products are:

1. **LIDAR Raw Time Series Laser Link Timing Data**: Time-series ASCII DSV table of raw data in the Laser Link mode. The data source is AOCSM telemetry.
2. **LIDAR Raw Time Series Range Data**: Time-series ASCII DSV table of raw data in the nominal ranging mode. The data source is AOCSM telemetry.
3. **LIDAR Raw Time Series Low Resolution (HK) Range Data**: Time-series ASCII DSV table of raw data in the nominal ranging mode. Only range data is calibrated and calculated on board. The data source is HK telemetry.
4. **LIDAR Raw Time Series Dust Count Data**: Time-series ASCII DSV table of raw data in the Dust Count mode. The data source is NAVSENS telemetry.
5. **LIDAR Partially Processed Time Series Laser Link Timing Data**: Time-series ASCII DSV table of timing data for the Laser Link experiment. This data is derived from LIDAR Raw Time Series Laser Link Timing Data. Only the observation epoch is calibrated.
6. **LIDAR Calibrated Time Series Laser Link Intensity Data**: Time-series ASCII DSV table of receiving/transmitting intensity data for the Laser Link experiment. This data is derived from LIDAR Raw Time Series Range Data and LIDAR Raw Time Series Low Resolution (HK) Range Data.
7. **LIDAR Calibrated Time Series Range Data**: Time-series ASCII DSV tables of LIDAR-measured range data in physical unit and related telemetry data. This data is derived from LIDAR Raw Time Series Range Data. Files are produced at a rate of one per day.
8. **LIDAR Calibrated Time Series Low Resolution (HK) Range Data**: Time-series ASCII DSV tables of LIDAR-measured range data in physical unit and related telemetry data. This data is derived from LIDAR Raw Time Series Low Resolution (HK) Range Data. Files are produced at a rate of one per day.
9. **LIDAR Calibrated Time Series Dust Count Data**: Time-series ASCII DSV tables of LIDAR dust count, threshold, wait distance. All values are in physical units. This data is derived from LIDAR Raw Time Series Dust Count Data. Files are produced at a rate of one per day when the dust count mode is in operation.
10. **LIDAR Derived Time Series Topography**: Time-series ASCII DSV tables of topography expressed by LIDAR footprint coordinates which are obtained from position of the target and navigation data of the spacecraft with L1b ranging data in physical units. This data is derived from LIDAR Calibrated Time Series Range Data. Files are produced after the asteroid rotational parameters are available.
11. **LIDAR Derived Time Series Low Resolution (HK) Topography**: Time-series ASCII DSV tables of topography expressed by LIDAR footprint coordinates which are obtained from position of the target and navigation data of the spacecraft with L1b ranging data in physical units. This data is derived from LIDAR Calibrated Time Series Low Resolution (HK) Range Data. Files are produced after the asteroid rotational parameters are available.
12. **LIDAR Derived Time Series Dust Count Data with Positions**: Time-series ASCII DSV tables of LIDAR dust count, observation start and end positions in the asteroid-fixed coordinates, and spacecraft position in the asteroid-fixed coordinates. All values are in physical units. This data is derived from LIDAR Calibrated Time Series Dust Count Data. Files are produced after the asteroid rotational parameters are available.
13. **LIDAR Derived Time Series Albedo Data**: Time-series ASCII DSV tables of LIDAR albedo value expressed by LIDAR footprint coordinates, which are obtained from the position of the target and navigation data of the spacecraft with LIDAR Calibrated Time Series Range Data in physical units.

14. **LIDAR Derived Albedo Map**: ASCII DSV table of asteroid longitude, latitude, average albedo, and corrected sample standard deviation within 3˚-by-3˚ grids. This data is derived from LIDAR Derived Time Series Albedo Data. Files are produced at a rate of one per day.
15. **LIDAR Derived Spacecraft Trajectory SPICE SPK**: SPICE SPK of the spacecraft derived from LIDAR Calibrated Time Series Range Data and LIDAR Calibrated Time Series Low Resolution (HK) Range Data.

5.3 Data Processing

This section of the SIS provides general information about data product content, format, size, and production rate. The specifics of the data product formats are discussed in Section 6.

5.3.1 Data Processing Level

LIDAR will deliver raw, calibrated, and derived data to PDS. The raw data correspond to CODMAC level 2 and include time-ordered instrument science data that have been combined with derived data products such as shape model of the target asteroid and spacecraft position, to create calibrated time series data files. All grid data products are derived products as one or more datasets are combined to produce the product. The processing level of "L1b" means that the time tags are verified, with potential 1 second offset may still remain (See section 5.3.2.2.1). LIDAR data products and their processing levels are summarized in Table 3.

Table 3. LIDAR data product processing levels

	LIDAR Product	PDS4 Processing Level	LIDAR Processing Level
1	LIDAR Raw Time Series Laser Link Timing Data	Raw	L0
2	LIDAR Raw Time Series Range Data	Raw	L0
3	LIDAR Raw Time Series Low Resolution (HK) Range Data	Raw	L0
4	LIDAR Raw Time Series Dust Count Data	Raw	L0
5	LIDAR Partially Processed Time Series Laser Link Timing Data	Partially Processed	L1b
6	LIDAR Calibrated Time Series Laser Link Intensity Data	Calibrated	L1b
7	LIDAR Calibrated Time Series Range Data	Calibrated	L1b
8	LIDAR Calibrated Time Series Low Resolution (HK) Range Data	Calibrated	L1b
9	LIDAR Calibrated Time Series Dust Count Data	Calibrated	L1b
10	LIDAR Derived Time Series Topography	Derived	L2
11	LIDAR Derived Time Series Low Resolution (HK) Topography	Derived	L2
12	LIDAR Derived Time Series Dust Count Data with Positions	Derived	L2
13	LIDAR Derived Time Series Albedo Data	Derived	L3
14	LIDAR Derived Albedo map	Derived	L4
15	LIDAR Derived Spacecraft Trajectory SPICE SPK	Derived	-

5.3.2 Data Product Generation

5.3.2.1 Raw Data

Raw data is downlinked from the spacecraft and stored as sorted telemetry in the telemetry database called SIRIUS, operated by C-SODA (Science Satellite Operation and Data Archive Unit) at ISAS, JAXA.

LIDAR makes an observation in response to a command sent from its parent system, Attitude and Orbit Control Unit (AOCU), and generate 20-byte data to be transmitted back to AOCU. Note that this bundle does not include all the 20-byte data as Level 0 products, but only includes subset of the data that are necessary to generate calibrated products. Time interval between each observation (or data transmission) is set by an AOCU command, and the minimum interval is 1 second. The contents of the data are different depending on LIDAR observation modes (ranging, dust count, and laser link modes).

Eight types of data that vary slowly over time, such as instrument temperature and APD applied voltage, are written to the last 12 bits of the 20-byte data, once every eight times in a fixed order. This is called as sub-word and is used to reduce the data size. The time interval at which the certain data stored in the sub-word is updated is eight times the time interval of LIDAR observation that is set by a command. The previous value is carried over until the same sub-word is updated, which is one reason (but not the only reason) to set an undefined value of -99999 when creating L1b product. This situation happens at the beginning of the packet where the previous value is absent. It should be noted that the timing of the change in APD GAIN (see Table 16) is not necessarily synchronized with that of the change in received power intensity, because the APD GAIN value is generated based on the APD applied voltage stored in the sub-word. The eight types of data are (1) DN_APD_HV_FAR, (2) DN_APD_HV_NEAR, (3) DN_TEMP_RX_APD_FAR, (4) DN_TEMP_RX_APD_NEAR, (5) DN_TEMP_RX_PK_FAR, (6) DN_TEMP_RX_PK_NEAR, and (7) DN_TEMP_TX_PK in Table 11, and (8) upper 1 byte of 2 bytes of laser shot count which is not included in the archive.

There are three types of packets that contain LIDAR data, namely, AOCSM and NAVSENS packets from Attitude and Orbit Control System (AOCS), and HK packet in which housekeeping data is collected. Only the NAVSENS packet holds complete 20 bytes of LIDAR data, while the AOCSM and the HK packets contain a subset of the data. The data are downlinked in pre-selected packet combinations.

The AOCSM packet consists of data from the AOCS and includes selected part of the LIDAR science data for the past 16 seconds. Therefore, if the AOCSM packets of 16-second division are downlinked, every second of the science data can be obtained. It does not include the LIDAR instrument setting information. The LIDAR ranging data for science are mainly generated from the AOCSM packets.

The NAVSENS packet consists of data from AOCS and includes 20 bytes of complete LIDAR data for 1 second. The dust count data are generated from the NAVSENS packets.

The HK packet consists of the minimum data required to monitor the health of all onboard instruments and includes a selected subset of the LIDAR data for the past 1 second. The resolution of HK ranging data is degraded to 1 m because the Least Significant Bit (LSB) is truncated. The LIDAR ranging data from HK packets complement AOCSM packets when there is no valid data in the AOCSM packet or during the period when AOCSM packets are not downlinked. The HK packet is always downlinked from the spacecraft, but a slower division is selected when the downlink bit rate is low.

Sections from 6.2.1 to 6.2.4 describe the contents of the raw data from three packets of AOCSM, NAVSENS, and HK. TI_TIME and CMD_TI are time indicator to determine timing of events (see section 5.3.2.2.1). Data whose label starts with a string "DN_" are digital numbers which are converted to strings or physical quantities in L1b products. Some labels do not start with the string "DN_" even though they are digital numbers, which shows that they are copied to L1b product without any manipulation or just used for data selection purpose. Table 4 shows the relationships among the packets, the LIDAR modes, the L0 products, and the L1b products.

Table 4. Relationships among the packets, the LIDAR modes, the L0 and the L1b products.

Source packet	LIDAR mode	L0 product	L1b product
AOCSM	Laser link	LIDAR Raw Time Series Laser Link Timing Data	LIDAR Partially Processed Time Series Laser Link Timing Data
AOCSM	Ranging	LIDAR Raw Time Series Range Data	LIDAR Calibrated Time Series Laser Link Intensity Data
AOCSM and HK*	Ranging	LIDAR Raw Time Series Range Data	LIDAR Calibrated Time Series Range Data
HK	Ranging	LIDAR Raw Time Series Low Resolution (HK) Range Data	LIDAR Calibrated Time Series Low Resolution (HK) Range Data
NAVSENS	Dust count	LIDAR Raw Time Series Dust Count Data	LIDAR Calibrated Time Series Dust Count Data

* Temperature of laser diode is contained in HK packet.

5.3.2.2 Partially Processed and Calibrated Data

Raw data with DN values are converted to calibrated data with physical units by using polynomial coefficients stored in a conversion database. The status of the instrument is also reproduced from the telemetry data with the conversion database. All the data are labelled as one of ranging mode, dust count mode, or laser link mode with a status telemetry to describe the observational mode, then time-series Level 1 data files are created for the ranging mode and dust count mode. One pipeline software takes care of the above procedures. The data with the laser link mode are processed outside of the pipeline scheme, because the laser link experiments were conducted, as of this writing, only twice in 2015 and 2020 in the Earth swing-by periods.

5.3.2.2.1 Timing of events

This subsection describes timing of events, e.g., firing laser or receiving laser, that are common to all the time series data products. The timing of events is estimated from two time-indicators of TI_TIME and CMD_TI. The former indicates the time when the telemetry packet is generated. The latter indicates the time when a LIDAR command is issued, but it only includes lower 2 bytes of the TI. The TI_TIME is generated by Data Handling Unit (DHU) and the CMD_TI is generated by AOCU. Note that telemetry packet is generated at DHU after issuing command at AOCU, so TI of issuing command should be earlier than TI of packet generated time, i.e., TI_TIME. By combining upper 2 bytes of TI_TIME and CMD_TI (lower 2 bytes), one can estimate 4 bytes of TI for time of issuing command that is denoted as FULL_CMD_TI. If the lower 2 bytes of TI_TIME is smaller than CMD_TI, subtract 65536 from FULL_CMD_TI. This calculation is described by the following pseudo-code:

```
if (0x0000FFFF & TI_TIME) < CMD_TI:
    FULL_CMD_TI = (0xFFFF0000 & TI_TIME) + CMD_TI − 65536
else:
    FULL_CMD_TI = (0xFFFF0000 & TI_TIME) + CMD_TI
```

Using this TI and partition number, SCLK string is derived. Appropriate partition number for data based on the SPICE SCLK for Hayabusa2 is shown in Table 5. SCLK string is constructed by the partition number and the TI in decimal. One can convert the SCLK string into ephemeris seconds past J2000 (Ephemeris Time, ET) by scs2e_c() using the SPICE toolkit with the Hayabusa2 SCLK and LSK. Then one can convert ET into UTC by et2utc_c() of the SPICE C toolkit. If one wants to obtain ET from UTC string, utc2et_c() can be used. Conversion from ET into SCLK string can be done by sce2s_c() of the toolkit.

Table 5 Partition number depending on date

Partition number	Start Time	Stop Time
1	2014-12-02T21:20:02Z	2017-09-05T04:59:58Z
2	2017-09-05T04:59:58Z	2021-05-17T21:59:59Z
3	2021-05-17T21:59:59Z	

There is a delay between issuing the command and firing the laser that is divided into two parts; one is the delay in the delivery of the issued command to LIDAR and the other is the delay between laser diode triggering and laser emission. The former is estimated to be 3 ticks of TI with ±1 tick uncertainty where one tick of the TI is about 1/32 seconds. The latter is measured by 299792458 Hz counter. The measured laser emission delay is denoted as TIMING_TX, TIMING_START, and DUST_START_TIMING for ranging mode, laser link mode, and dust count mode, respectively. One AOCSM packet contains 16 seconds of LIDAR data that are distinguished by DUMP_NUM. The DUMP_NUM values of 1 and 16 correspond to the newest and the oldest data in the packet. These variables and events related to the laser shot is shown in Figure 1 for the dust count mode and the ranging mode where INTERVAL = 1 (shot interval = 1 second) is assumed, and shown in Figure 2 for the laser link mode.

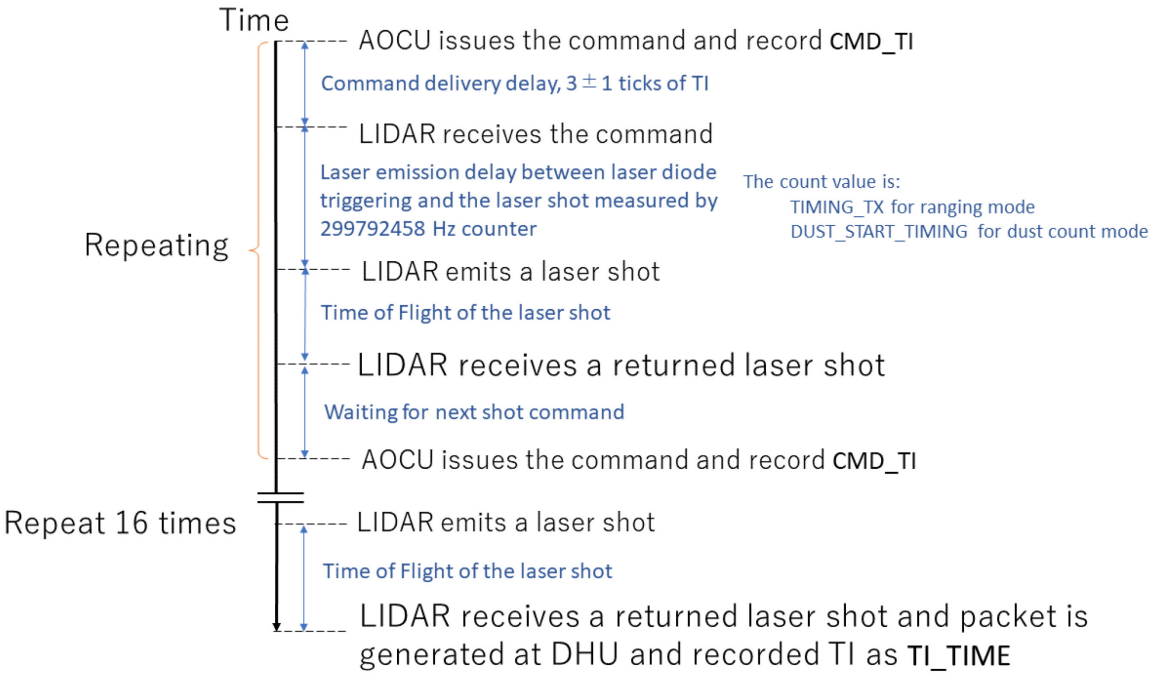

Figure 1 Timing chart of the laser shot events and recorded variables for ranging mode and dust count mode. The INTERVAL value is set to 1 is assumed for the ranging mode in this figure.

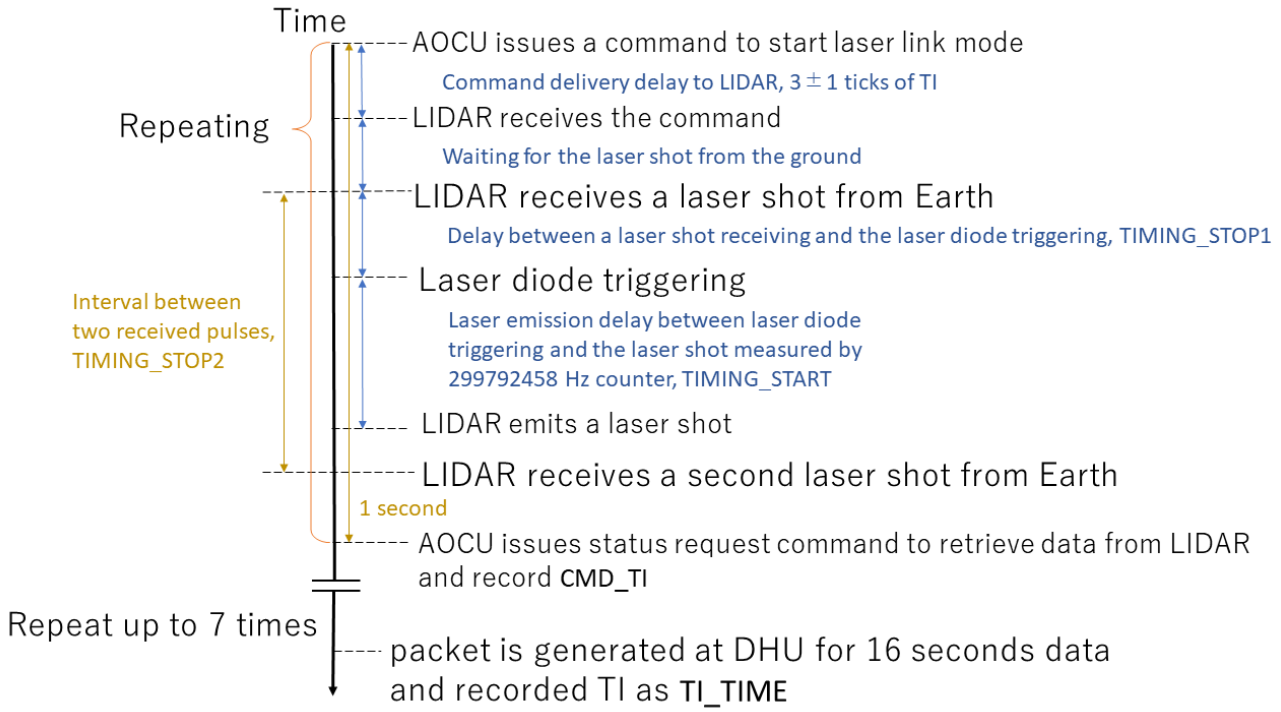

Figure 2 Timing chart of the laser shot events and recorded variables for laser link mode.

In the laser link mode, LIDAR starts waiting for laser pulses from the ground station by the specific laser link start command. This command changes the internal status of LIDAR but does not send any responses back to AOCU. Therefore, we send another command one second later to record TI (CMD_TI) for estimation of time when the laser link start command is issued.

For Laser Link Timing Data, TI of the time to start waiting for laser pulses from the ground is estimated by

$$(\text{FULL\_CMD\_TI} - (\text{DUMP\_NUM} - 1) * 32 + 3 - 32) \quad (1)$$

where the third term is delay time for the command to reach LIDAR and the fourth term is correction for the above mentioned one second delay. Using this TI and partition number, SCLK string (SCLK_CLOCK_STRING) is derived, and then the TI will be converted into UTC which is denoted as WAIT_START_TIME.

For Laser Link Intensity Data, TI of the time when LIDAR receives the laser shot command is estimated by

$$(\text{FULL\_CMD\_TI} - (\text{DUMP\_NUM} - 1) * 32 + 3) \quad (2)$$

where the third term is delay time for the command to reach LIDAR. Using this TI and partition number, SCLK_CLOCK_STRING is derived, and is converted to ET by using the SPICE toolkit with SCLK and LSK, which is further corrected for the laser emission delay to get the time when a laser pulse is shot (denoted as SHOT_TIME). The laser emission delay in seconds, calculated as TIMING_TX/299792458, is added to the ET that is converted to UTC.

For Time Series Range Data, if the value of INTERVAL is 1 (shot interval = 1 second), TI of the time when LIDAR receives the laser shot command is calculated as

$$(\text{FULL\_CMD\_TI} - (\text{DUMP\_NUM} - 1) * 32 + 3) \quad (3)$$

where the third term is delay time for the command to reach LIDAR. If the value of INTERVAL is 0 (shot interval = 32 seconds), the TI for laser shot time is calculated as

$$(\text{FULL\_CMD\_TI} + 3) \quad (4)$$

because in this case the dump number (DUMP_NUM) is meaningless. The TI is converted to ET by using the SPICE toolkit with SCLK and LSK, which is further corrected for the laser emission delay to get the time when a laser pulse is shot (denoted as SHOT_TIME). The laser emission delay in seconds, calculated as TIMING_TX/299792458, is added to the ET that is converted to UTC.

For Time Series Dust Count Data, shot interval is fixed to 1 second. The TI for laser shot time is calculated as Equation (4). The TI is converted to ET by using the SPICE toolkit with SCLK and LSK, which is further corrected for the laser emission delay to get the time when a laser pulse is shot (denoted as SHOT_TIME). The laser emission delay in seconds, calculated as DUST_START_TIMING /299792458, is added to the ET that is converted to UTC.

The LIDAR range data with 32-second repetition period is mainly downlinked by HK packet to save downlink resources. However, the laser shot time cannot be estimated from the HK packet alone because that packet does not contain the time when the LIDAR command is sent from AOCU (CMD_TI) nor the time between laser diode triggering and the emission of the laser (TIMING_TX). In order to know the laser shot time of the observation at every 32 second, we record the telemetry data to AOCSM packet for at least one laser shot at the beginning and/or the end of the observation. We regarded the laser shot time determined by the AOCSM packet as that of the HK packet. The subsequent laser shot times of HK data are given by extrapolating the AOCSM-determined shot time where the observation interval is assumed to be (32 ticks of TI)*32 (about 32 seconds). See section 5.3.2.2.5 for details.

5.3.2.2.2 LIDAR Partially Processed Time Series Laser Link Timing Data

The time when LIDAR starts waiting for laser pulses from a ground station is calibrated. See section 5.3.2.2.1 for details of the timing of events.

The data that meet the following conditions for LIDAR Raw Time Series Laser Link Timing Data product are retained in this product for laser link experiments in 2015:

LIDAR_MODE = 2 [OPT (laser link)]

and VAL_ST = 1 [valid]

and STOP2_PLS_DET = 1 [2nd pulse detected]

and (TIMING_STOP2 < 25000 or TIMING_STOP2 > 30000)

Note that only WAIT_START_TIME, the time to start waiting for the laser pulses from a ground station, is calibrated.

5.3.2.2.3 LIDAR Calibrated Time Series Laser Link Intensity Data

Although this product is classified into laser link product, the LIDAR mode is set to “ranging” to get intensities of transmitting/receiving laser from AOCSM packet during the laser link experiment. Please refer to descriptions related to the laser intensity in section 5.3.2.2.4.

5.3.2.2.4 LIDAR Calibrated Time Series Range Data

The observed range is calculated from timing difference between transmission and reception with a bias being corrected for. The bias consists of internal system delay and peak correction. The latter is necessary because the reception timing is detected when received signal exceeds threshold, which

gives shorter range than it actually is. The reference of LIDAR range observation is the instrument's mounting plane.

The range data for the far optics L_{far}, that is denoted as RANGE_FAR in Table 16, is calculated as follows:

$$L_{\mathrm{far}}\,[\mathrm{m}] = \alpha_{\mathrm{far}} \times dL_{\mathrm{far}} \times \left(C_{\mathrm{RX,far,DN}} - C_{\mathrm{TX,DN}}\right) + K_{\mathrm{bias,far}} \tag{5}$$

$$K_{\mathrm{bias,far}} = \Delta R_{\mathrm{SD}} + \Delta R_{\mathrm{peak,far}} \tag{6}$$

$$\Delta R_{\mathrm{peak,far}} = \beta_{\mathrm{far},1} \times P_{\mathrm{far,DN}} + \beta_{\mathrm{far},0} \tag{7}$$

Similarly, the range data for the near optics L_{near} (RANGE_NEAR in Table 16) is calculated as follows:

$$L_{\mathrm{near}}\,[\mathrm{m}] = \alpha_{\mathrm{near}} \times dL_{\mathrm{near}} \times \left(C_{\mathrm{RX,near,DN}} - C_{\mathrm{TX,DN}}\right) + K_{\mathrm{bias,near}} \tag{8}$$

$$K_{\mathrm{bias,near}} = \Delta R_{\mathrm{SD}} + \Delta R_{\mathrm{peak,near}} \tag{9}$$

$$\Delta R_{\mathrm{peak,near}} = \beta_{\mathrm{near},1} \times P_{\mathrm{near,DN}} + \beta_{\mathrm{near},0} \tag{10}$$

Note that when $\left(C_{\mathrm{RX,far,DN}} - C_{\mathrm{TX,DN}}\right)$ is negative, it is replaced by $\left(C_{\mathrm{RX,far,DN}} - C_{\mathrm{TX,DN}}\right) + 2^{17}$, and the same applies to $\left(C_{\mathrm{RX,near,DN}} - C_{\mathrm{TX,DN}}\right)$. See Table 6 for detailed description of each parameter.

If RX_PLS_DET_FAR is 0, the returned pulse is not detected by the far optics, then RANGE_FAR is set to -99999. Similarly, if RX_PLS_DET_NEAR is 0, the returned pulse is not detected by the near optics, then RANGE_NEAR is set to -99999.

The conversion equation for transmitted energy I_{TX} in J (INTENS_TX in Table 15 and Table 16) is as follows:

$$I_{\mathrm{TX}} = 2.220 \times 10^{-4} \times P_{\mathrm{TX,DN}} + 3.698 \times 10^{-4} \times T_{\mathrm{LD}} - 2.160 \times 10^{-2} \tag{11}$$

where $P_{\mathrm{TX,DN}}$ is telemetry data of transmitted pulse intensity and T_{LD} is temperature of laser diode. T_{LD} is calculated as

$$T_{\mathrm{LD}} = 5.21132734 \times 10^{-1} \times T_{\mathrm{LD,DN}} - 5.319815526 \times 10^{1} \tag{12}$$

Note that $T_{\mathrm{LD,DN}}$ comes from HK packet, not from AOCSM packet. First, calculate T_{LD} at TI_TIME by Equation (12). Second, get T_{LD} at SHOT_TIME by linearly interpolating the HK-based T_{LD} values at TI_TIME. Third, calculate I_{TX} by Equation (11) with the interpolated T_{LD}. Note also that when calculating the transmitted energy I_{TX} in LIDAR Calibrated Time Series Range Data, temperature of laser diode T_{LD} is rounded off to third decimal place in degC, which may affect the value of I_{TX} at sixth decimal digit in J.

The peak voltage (in V) of receiving APD for the FAR optics $I_{\mathrm{RX,far}}$ (INTENS_RX_FAR in Table 15, Table 16, and Table 17) is calculated as follows:

$$\begin{aligned} I_{\mathrm{RX,far}} = {} & -1.09891 \times 10^{-10} \times {P_{\mathrm{far,DN}}}^{4} + 1.22333 \times 10^{-7} \times {P_{\mathrm{far,DN}}}^{3} \\ & -6.65067 \times 10^{-6} \times {P_{\mathrm{far,DN}}}^{2} + 1.39357 \times 10^{-3} \times P_{\mathrm{far,DN}} \\ & +2.8697 \times 10^{-2} \end{aligned} \tag{13}$$

Note that these conversion equations are slightly different from those in Yamada et al. (2017) where the transmitted energy and the peak voltage of APD are denoted as $E_{\mathrm{T}}(D_{\mathrm{T}})$ and $R_{\mathrm{S}}(D_{\mathrm{R}})$, respectively. Although Yamada et al. (2017) describes energy calibration for the FAR optics only, peak voltage (in V) for the NEAR optics $I_{\mathrm{RX,near}}$ (INTENS_RX_NEAR in Table 16 and Table 17) is calculated as follows:

Table 6. Description of parameters that are used for calculating observed range value.

Name	Classification	Notation	Value	Unit	Remarks
Transmission timing	Telemetry	$C_{\mathrm{TX,DN}}$			Count value, TIMING_TX in Table 11 and Table 16
Far reception timing	Telemetry	$C_{\mathrm{RX,far,DN}}$			Count value, TIMING_RX_FAR in Table 13 and Table 16
Far range	Variable	L_{far}		m	RANGE_FAR in Table 16
Far range resolution	Constant	dL_{far}	0.5	m	
Correction coefficient for crystal oscillator frequency	Constant	α_{far}	1.0000125		Measured with PFM. For far range counter.
Measurement bias for far optics	Variable	$K_{\mathrm{bias,far}}$		m	
Peak correction for far optics	Variable	$\Delta R_{\mathrm{peak,far}}$		m	
Peak value of signal received by far optics	Telemetry	$P_{\mathrm{far,DN}}$			0-255, DN_INTENS_RX_FAR in Table 11 and Table 12
Peak correction coefficient for far optics (slope)	Constant	$\beta_{\mathrm{far},1}$	0.0127		Measured with PFM
Peak correction coefficient for far optics (intercept)	Constant	$\beta_{\mathrm{far},0}$	-0.35		Measured with PFM
Near reception timing	Telemetry	$C_{\mathrm{RX,near,DN}}$			Count value, TIMING_RX_NEAR in Table 13 and Table 16
Near range	Variable	L_{near}		m	RANGE_NEAR in Table 16
Near range resolution	Constant	dL_{near}	0.5	m	
Correction coefficient for crystal oscillator frequency	Constant	α_{near}	1.0000125		Measured with PFM. For near range counter.
Measurement bias for near optics	Variable	$K_{\mathrm{bias,near}}$		m	
Peak correction for near optics	Variable	$\Delta R_{\mathrm{peak,near}}$		m	
Peak value of signal received by near optics	Telemetry	$P_{\mathrm{near,DN}}$			0-255, DN_INTENS_RX_NEAR in Table 11 and Table 12
Peak correction coefficient for near optics (slope)	Constant	$\beta_{\mathrm{near},1}$	0.0121		Measured with PFM
Peak correction coefficient for near optics (intercept)	Constant	$\beta_{\mathrm{near},0}$	0		Measured with PFM
Internal system delay	Constant	ΔR_{SD}	-3.324	m	Measured with PFM

$$I_{\mathrm{RX,near}} = -1.16150 \times 10^{-9} \times {P_{\mathrm{near,DN}}}^{4} + 4.78438 \times 10^{-7} \times {P_{\mathrm{near,DN}}}^{3} - 4.53788 \times 10^{-5} \times {P_{\mathrm{near,DN}}}^{2} + 3.06464 \times 10^{-3} \times P_{\mathrm{near,DN}} + 1.61958 \times 10^{-2} \quad (14)$$

The pipeline forces the value of INTENS_RX_FAR/NEAR to zero when DN_INTENS_RX_FAR/NEAR is zero.

The APD gain parameter for the FAR range finder (APD_GAIN_FAR in Table 16) is set as follows:

```
if (DN_APD_HV_FAR > 2700) then
    APD_GAIN_FAR = 8
else if (DN_APD_HV_FAR > 2300) then
    APD_GAIN_FAR = 4
else if (DN_APD_HV_FAR > 1600) then
    APD_GAIN_FAR = 2
else if (DN_APD_HV_FAR > 1000) then
    APD_GAIN_FAR = 1
else
    APD_GAIN_FAR = -99999
endif
```

If DN_APD_HV_FAR ≤ 1000, value of APD_GAIN_FAR is set to -99999 which means that APD is not ready for observation. The same applies to the APD gain parameter for the NEAR range finder, APD_GAIN_NEAR in Table 16, of which value depends on DN_APD_HV_NEAR.

Described below are conversion equations for temperatures from telemetry data ($T_{\mathrm{APD,far,DN}}$, $T_{\mathrm{APD,near,DN}}$, $T_{\mathrm{RX,far,DN}}$, $T_{\mathrm{RX,near,DN}}$, and $T_{\mathrm{TX,DN}}$). The temperature (in degC) of APD in the FAR range finder $T_{\mathrm{RX,APD,far}}$ (TEMP_RX_APD_FAR in Table 16) is calculated from $T_{\mathrm{APD,far,DN}}$ (DN_TEMP_RX_APD_FAR in Table 11) as follows:

$$T_{\mathrm{RX,APD,far}} = 3.432 \times 10^{-1} \times T_{\mathrm{APD,far,DN}} - 3.902 \times 10^{1} \quad (15)$$

If the calculated value is less than -10 degC or greater than 45 degC, -99999 is set as invalid constant.

The temperature (in degC) of APD in the NEAR range finder $T_{\mathrm{RX,APD,near}}$ (TEMP_RX_APD_NEAR in Table 16) is calculated from $T_{\mathrm{APD,near,DN}}$ (DN_TEMP_RX_APD_NEAR in Table 11) as follows:

$$T_{\mathrm{RX,APD,near}} = 3.461 \times 10^{-1} \times T_{\mathrm{APD,near,DN}} - 4.013 \times 10^{1} \quad (16)$$

If the calculated value is less than -10 degC or greater than 45 degC, -99999 is set as invalid constant.

The temperature (in degC) of peak-detection circuit in the FAR range finder $T_{\mathrm{RX,PK,far}}$ (TEMP_RX_PK_FAR in Table 16) is calculated from $T_{\mathrm{RX,far,DN}}$ (DN_TEMP_RX_PK_FAR in Table 11) as follows:

$$T_{\mathrm{RX,PK,far}} = -4.59111 \times 10^{-6} \times {T_{\mathrm{RX,far,DN}}}^{4} + 3.17357 \times 10^{-3} \times {T_{\mathrm{RX,far,DN}}}^{3} - 8.10877 \times 10^{-1} \times {T_{\mathrm{RX,far,DN}}}^{2} + 8.92789 \times 10^{1} \times T_{\mathrm{RX,far,DN}} - 3.47151 \times 10^{3} \quad (17)$$

If the calculated value is less than -10 degC or greater than 70 degC, -99999 is set as invalid constant.

The temperature (in degC) of peak-detection circuit in the NEAR range finder $T_{\mathrm{RX,PK,near}}$ (TEMP_RX_PK_NEAR in Table 16) is calculated from $T_{\mathrm{RX,near,DN}}$ (DN_TEMP_RX_PK_NEAR in Table 11) as follows:

$$T_{\mathrm{RX,PK,near}} = -3.4266 \times 10^{-5} \times {T_{\mathrm{RX,near,DN}}}^{3} + 2.4869 \times 10^{-2} \times {T_{\mathrm{RX,near,DN}}}^{2} - 6.8412 \times T_{\mathrm{RX,near,DN}} + 6.4053 \times 10^{2} \quad (18)$$

If the calculated value is less than -10 degC or greater than 70 degC, -99999 is set as invalid constant.

The temperature (in degC) of peak-detection circuit in the laser transmitter $T_{\mathrm{TX,PK}}$ (TEMP_TX_PK in Table 16) is calculated from $T_{\mathrm{TX,DN}}$ (DN_TEMP_TX_PK in Table 11) as follows:

$$T_{\mathrm{TX,PK}} = 6.9535 \times 10^{-3} \times {T_{\mathrm{TX,DN}}}^{2} - 3.7850 \times T_{\mathrm{TX,DN}} + 4.7054 \times 10^{2} \quad (19)$$

If the calculated value is less than -10 degC or greater than 70 degC, -99999 is set as invalid constant.

The data that meet the following conditions are retained in this product:

LIDAR_MODE = 0 [MEAS (ranging)]

and VAL_ST = 1 [valid]

and STOP_OVF = 0 [no overflow]

and TX_PLS_DET = 1 [transmitted pulse detected]

and (RX_PLS_DET_FAR = 1 or RX_PLS_DET_NEAR = 1) [received pulse detected]

The LIDAR team visually checks the calibrated time series range data and manually removes abnormal values. The L1b time series range data is subjected to this filtering process before estimating spacecraft trajectory (section 5.3.2.3.6) that requires the L1b data. Note that temporal profiles of the LIDAR ranges sometimes show saw-toothed patterns when LIDAR is directed toward the limb of the asteroid, which are not removed but are retained as they are. Figure 3 shows an example on September 29, 2019.

The active telescope is not exclusive, and both FAR and NEAR telescopes can be simultaneously activated (i.e., high-voltage ON). This happens during descent operations (roughly 1000 m > altitude > 300 m). The AOCSM has two range slots for FAR and NEAR both of which can have non-zero values. Even when high-voltage is OFF, the received intensity (INTENS_RX_FAR/NEAR) can have non-zero values because it is possible for a sensor semiconductor to produce a signal in response to incoming light.

A bunch of 16-second range data are missing every 32 seconds between 2019-03-20T20:20:00Z and 2019-03-21T18:50:00Z. It should be noted that FAR telescope was incorrectly selected between 2019-05-16T02:24:59.374842Z and 2019-05-16T02:34:22.366763Z. The LIDAR range measurements for NEAR telescope should be used for this period.

Although the headmost time of L0 packet is after 00:00:00, the packet can contain data up to 16 seconds ago, sometimes crossing the boundary of the day. On the other hand, we re-shaped the L1b data so as not to straddle the boundary of the day. The final L1b product contains data between 00:00:00.000000Z and 23:59:59.999999Z. This post-processing was done outside the pipeline. Sometimes two L0 files are needed to create a L1b file. For example, the pre-midnight part of hyb2_ldr_l0_aocsm_range_ts_20190530_v01.csv is used to create the ending part of hyb2_ldr_l1b_aocsm_range_ts_20190529_v102.csv.

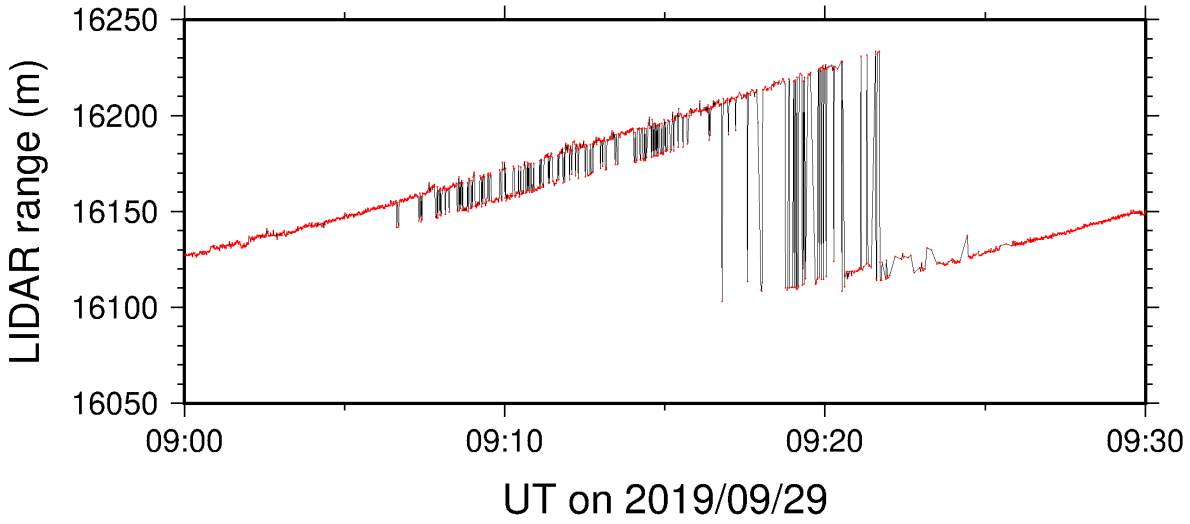

Figure 3. An example of saw-toothed LIDAR range profile.

5.3.2.2.5 LIDAR Calibrated Time Series Low Resolution (HK) Range Data

Conversion equations for this product are the same as those described in section 5.3.2.2.4.

The data that meet the following conditions are retained in this L1b product:

LIDAR_MODE = 0 [MEAS (ranging)]

and ((DN_RX_TELESCOPE = 0 and RANGE >200 m and RANGE < 30000 m)

or (DN_RX_TELESCOPE = 1))

and (Laser transmission is ON)

Because HK telemetry does not contain TX_PLS_DET, the status of laser transmission is evaluated based on AOCSM telemetry. The AOCSM telemetry is obtained when we start/stop the LIDAR ranging or change the observation interval (1 sec or 32 sec) so that we can infer whether laser transmission is ON or OFF during certain period of data acquisition by HK telemetry.

The laser shot time is estimated by supplementing the necessary information with AOCSM telemetry. Let us take data of July 14, 2018 as an example below.

The followings are the last three lines from hyb2_ldr_l0_aocsm_range_ts_20180714_v01.csv.

14:28:27,337B53EF,10,52C4,0,0,0,1,1,0,1,0,66992,0,26592,0,0,130,2821,17,179,1,183,184,184
14:28:51,337B56EF,2,56C4,0,0,0,1,1,0,1,0,66918,0,26520,3,0,116,2821,17,179,1,183,184,184
14:29:23,337B5AEF,2,5AC4,0,0,0,1,1,0,1,0,67008,0,26616,1,0,125,2822,17,179,1,183,184,184

The TI of the laser shot time for the last entry is 337B5AC4 + 3 = 337B5AC7. We predict shot times beyond the last entry by assuming a shot interval of 32*(32 TI). Because 32*32 (decimal) = 1024 (decimal) = 400 (hexadecimal), the predicted TIs are:

337B5AC7 (= 14:29:22.033601)
337B5EC7 (= 14:29:54.033192)
337B62C7 (= 14:30:26.032784)
337B66C7 (= 14:30:58.032375)
337B6AC7 (= 14:31:30.031996)

The corresponding part from hyb2_ldr_l0_hk_range_ts_20180714_v01.csv is as follows:

14:29:22,337B5AE0,0,0,20192,1,0,145
14:29:30,337B5BE0,0,0,20192,1,0,146
14:29:46,337B5DE0,0,0,20192,1,0,146
14:30:02,337B5FE0,0,0,20190,3,0,146
14:30:18,337B61E0,0,0,20190,3,0,146
14:30:34,337B63E0,0,0,20190,2,0,147
14:30:50,337B65E0,0,0,20190,2,0,147
14:31:06,337B67E0,0,0,20200,0,0,147
14:31:38,337B6BE0,0,0,20194,1,0,145
14:31:54,337B6DE0,0,0,20194,1,0,144

The alternate yellow and green hatchings indicate data blocks in which RANGE, DN_INTENS_RX_FAR, and DN_INTENS_RX_NEAR (columns 5-7) are the same. We pick up the headmost data from each block as the source of L1b data. We find predicted TI of shot time (e.g., 337B5AC7) that is close to TI_TIME in the headmost data (e.g., 337B5AE0). The predicted TI is converted to ET by the SPICE that is further corrected for the emission delay by adding TIMING_TX/299792458 (in seconds). The ET is converted to UTC to form the final SHOT_TIME. The TIMING_TX comes from the AOCSM packet (e.g., 26616). The followings are the corresponding part of hyb2_ldr_l1b_hk_range_ts_20180714_v102.csv that is time-tagged as mentioned above.

2018-07-14T14:29:54.033281Z,337B5FE0,FAR,20190.0,32.821,0.000
2018-07-14T14:30:26.032872Z,337B63E0,FAR,20190.0,31.459,0.000
2018-07-14T14:30:58.032464Z,337B67E0,FAR,20200.0,0.000,0.000
2018-07-14T14:31:30.032055Z,337B6BE0,FAR,20194.0,30.084,0.000

The LIDAR team visually checks the calibrated time series low resolution range data and manually removes abnormal values. The L1b time series range data is subjected to this filtering process that is necessary for estimating spacecraft trajectory (section 5.3.2.3.6). We excluded L1b HK range entries that have duplicated period with AOCSM temporal coverage, because AOCSM has higher range accuracy as well as more reliable time tags.

5.3.2.2.6 LIDAR Calibrated Time Series Dust Count Data

The detection threshold for far optics (DN_THRESHOLD) is converted to mV by Table 7. The distance between the spacecraft to the start point of the dust observation in the line-of-sight direction D_{wait} (WAIT_DISTANCE in Table 18) in meter is calculated as

$$D_{\text{wait}} = D_{\text{wait,DN}} \times 150 \tag{20}$$

The data that meet the following conditions are retained in this product:

LIDAR_MODE = 1 [DUST]

and DN_RX_TELESCOPE = 0 [far]

and APD_HV_PWR_FAR = 1 [high voltage on]

and RANGE_ENA = 1 [ranging enable]

and DUST_COUNT_ENA = 1 [dust count enable]

and DUST_START_TIMING ≠ 0

Table 7. Conversion table for threshold of the far optics.

DN_THRESHOLD (decimal)	THRESHOLD (mV)
63	4.3
58	9.3
34	14.4
40	27.0
8	37.3

5.3.2.3 Derived Data

5.3.2.3.1 LIDAR Derived Time Series Topography

The time series topography is a sequence of LIDAR footprint positions expressed in asteroid-centered body-fixed rotating frame. Spacecraft trajectory is necessary in order to create this data product, and the LIDAR range data themselves are used to estimate the trajectory by combining with an image-based shape model (see section 5.3.2.3.6).

SHOT_TIME in Table 19 is a copy of that in LIDAR Calibrated Time Series Range Data (Table 16). RANGE in Table 19 is also a copy of RANGE_FAR or RANGE_NEAR in LIDAR Calibrated Time Series Range Data (Table 16) depending on the selected optics. See section 5.5 for an exception on May 16, 2019. The LIDAR footprint position at SHOT_TIME t is computed as

$$\boldsymbol{F}(t) = \boldsymbol{S}(t) + \hat{\boldsymbol{l}}(t)R(t) \tag{21}$$

where $\boldsymbol{F}(t)$ is footprint position vector, $\boldsymbol{S}(t)$ is spacecraft position vector, $\hat{\boldsymbol{l}}(t)$ is LIDAR pointing unit vector (spacecraft attitude plus LIDAR alignment), and $R(t)$ is observed LIDAR range. All the vectors are described in asteroid-centered body-fixed rotating frame. The spacecraft position vector is obtained from SPICE SPK of the lidar-derived trajectory, the spacecraft attitude is obtained from SPICE CK, and the LIDAR alignment information is obtained from SPICE FK. In section 6.2.10, $\boldsymbol{F}(t)$ is described both in rectangular coordinates as (TOPO_X, TOPO_Y, TOPO_Z) and in longitude/latitude/height coordinates as (TOPO_LONGITUDE, TOPO_LATITUDE, TOPO_HEIGHT), and $\boldsymbol{S}(t)$ is described in rectangular coordinates as (SC_POS_X, SC_POS_Y, SC_POS_Z).

It is known that the LIDAR time tag can have 1 second ambiguity. As is discussed in Matsumoto et al. (2020), the time tag error is not critical for nominal observations but is brought into sight when the spacecraft attitude is rapidly scanned. All the scan observations were subjected to the time tag check and we have detected the time tag error for two scan observations on 19 July 2018 and 25 October 2019. The time tags for these two scan observations have already been rectified.

5.3.2.3.2 LIDAR Derived Time Series Low Resolution (HK) Topography

The HK-related topography products are generated in the same way as described in section 5.3.2.3.1, but the source of SHOT_TIME and RANGE in Table 20 is LIDAR Calibrated Time Series Low Resolution (HK) Range Data (Table 17). This product is generated only during the period when AOCSM telemetry is not available.

5.3.2.3.3 LIDAR Derived Time Series Dust Count Data with Positions

The items SHOT_TIME, THRESHOLD, and DUST_CNT_01 in Table 21 are copies of those in LIDAR Calibrated Time Series Dust Count Data (Table 18). The coordinates of dust count starting position

(DUST_START_X, DUST_START_Y, and DUST_START_Z in in Table 21) are calculated by replacing R with D_{wait} in Equation (21). Similarly, the coordinates of dust count ending position (DUST_END_X, DUST_END_Y, and DUST_END_Z in in Table 21) are calculated by replacing R with $D_{\mathrm{wait}} + 1000$ (m) in Equation (21).

Note that the calculations using the SPICE toolkit were done with the old Ryugu's PCK, ryugu_v08.tpc containing Ryugu's orientation parameters obtained by the shape model version 20181109, instead of the latest version, ryugu_v10.tpc.

5.3.2.3.4 LIDAR Derived Time Series Albedo Data

The time series albedo data is a sequence of normal albedos at LIDAR footprints along the spacecraft trajectory. The albedos are principally calculated as a ratio of energy received by the APD, E_{obs}, and energy transmitted by LIDAR, E_{T}, taking into account geometric attenuation. However, because the surface of Ryugu is very rough, careful considerations such as return pulse waveform and reflection laws are necessary (Yamada et al., 2022).

The relationship of E_{obs}, E_{T}, and the normal albedo, ρ (ALBEDO in Table 22) is given by Equation (5) of Yamada et al. (2022).

$$E_{\mathrm{obs}} = \frac{E_{\mathrm{T}}}{\pi} \rho \, \beta \int_0 dt \int_{\mathrm{footprint}} ds_{xy} \, \xi_{xy}(i_{xy}, i_{xy}) \varepsilon_{xy} \frac{A_0}{{L_{xy}}^2} \, \tau\left(t - \frac{2L_{xy}}{c}\right) \tag{22}$$

where β is the transmissivity of the optical system of the receiver and is 0.678 (Yamada et al., 2022). The laser footprint corresponds to the FOV of the FAR telescope (Table 2); xy denotes the position within the FOV; i_{xy} is the incident angle at xy and is dependent on local topography; ds_{xy} is the small area within the footprint; t is the time from the beginning of laser transmission; L_{xy} is the distance between xy and the LIDAR telescope; and c is the speed of light. A_0 is the aperture area of the receiving FAR telescope, 0.0095 m^2, and ${A_0}/{{L_{xy}}^2}$ is the solid angle of the aperture viewed from xy. The function $\tau(t)$ represents the time-wise intensity profile of the transmitted laser beam and is normalized over the beam divergence. The time delay of laser reception from reflection is considered. ξ_{xy} is the disk function. ε_{xy} is the normalized beam pattern of the transmitted laser pulse, and its integration within the beam divergence is one (Mizuno et al., 2017; Yamada et al., 2022).

According to Yamada et al. (2022), the reflection property of Ryugu is better simulated by Lommel-Seeliger law than Lambert law, indicating that $\xi_{xy}(i_{xy}, i_{xy})$ of Equation (22) equals one (see also Equation (11) of Yamada et al., 2022). Their finding makes Equation (22) simple.

$$\begin{aligned}
E_{\mathrm{obs}} &= \frac{E_{\mathrm{T}}}{\pi} \rho \, \beta \int_0 dt \int_{\mathrm{footprint}} ds_{xy} \, \varepsilon_{xy} \frac{A_0}{{L_{xy}}^2} \, \tau\left(t - \frac{2L_{xy}}{c}\right) \\
&= \frac{E_{\mathrm{T}}}{\pi} \rho \, \beta \int_{\mathrm{footprint}} ds_{xy} \, \varepsilon_{xy} \frac{A_0}{{L_{xy}}^2} \int_0 dt \; \tau\left(t - \frac{2L_{xy}}{c}\right) \\
&= \frac{E_{\mathrm{T}}}{\pi} \rho \, \beta \int_{\mathrm{footprint}} ds_{xy} \, \varepsilon_{xy} \frac{A_0}{{L_{xy}}^2} \\
&\cong \frac{E_{\mathrm{T}}}{\pi} \rho \, \beta \frac{A_0}{\bar{L}^2} \int_{\mathrm{footprint}} ds_{xy} \, \varepsilon_{xy} \\
&= \frac{E_{\mathrm{T}}}{\pi} \rho \, \beta \frac{A_0}{\bar{L}^2} \, \bar{\varepsilon}
\end{aligned} \tag{23}$$

In the above Equation (23), we first exchange the order of integrations in space and time. For a sufficiently long integration time that contains a whole return pulse, the temporal integration of

normalized $\tau\left(t-\frac{2L_{xy}}{c}\right)$ equals one regardless of L_{xy}. Next, L_{xy} is approximately replaced by the range, $\bar{L}$ (RANGE_FAR in Table 16). This approximation causes errors due to the footprint size and topography within a footprint. The former is less than 0.1% as FOV is 1.5 mrad (Table 2). The latter is a few % at most for the albedo observation from the lowest altitude, which is about 1000 m, assuming that the roughness within a footprint is a few m. These errors are smaller than the estimated overall error of ρ of 15.3% (Yamada et al., 2022). Finally, we substitute the utilization ratio of laser energy, $\bar{\varepsilon}$, for the spatial integration of ε_{xy}. $\bar{\varepsilon}$ is given by Equation (17) of Yamada et al. (2017) as 0.409 $\pm$ 0.017. Note that $\bar{\varepsilon}$ is smaller than one because ε_{xy} is normalized over the 2.4-mrad wide beam divergence while the spatial integration is limited within the FOV (Mizuno et al., 2017; Yamada et al., 2022).

The formulae to calculate E_{obs} and E_{T} are given by Equations (9) and (12) in Yamada et al. (2022).

$$E_{\mathrm{obs}}\left(P_{\mathrm{far,DN}}\right)=\frac{10}{M}\left(8.381\times10^{-25}{P_{\mathrm{far,DN}}}^{5}-7.447\times10^{-22}{P_{\mathrm{far,DN}}}^{4}+2.225\times10^{-19}{P_{\mathrm{far,DN}}}^{3}\right.$$
$$\left.-2.337\times10^{-17}{P_{\mathrm{far,DN}}}^{2}+1.194\times10^{-15}P_{\mathrm{far,DN}}-5.399\times10^{-15}\right) \quad (24)$$

$$E_{T}\left(P_{\mathrm{TX,DN}}\right)=-6.03859\times10^{-7}{P_{\mathrm{TX,DN}}}^{3}+2.36165\times10^{-4}{P_{\mathrm{TX,DN}}}^{2}$$
$$-3.04973\times10^{-2}P_{\mathrm{TX,DN}}+1.31578 \quad (25)$$

where both E_{obs} and E_{T} are in J. M is the multiplication factor (see Section 5.1) whose corresponding gain (APD_GAIN_FAR in Table 16) and responsivity are explained in detail for INTENS_RX_FAR in Table 16; $P_{\mathrm{far,DN}}$ is the peak value of signal received by far optics in digital unit (DU) (DN_INTENS_RX_FAR in Table 11 and 12; see also Table 6); and $P_{\mathrm{TX,DN}}$ is the peak value of transmitted signal in DU (DN_INTENS_TX in Table 11; see 5.3.2.2.4). $P_{\mathrm{far,DN}}$ and $P_{\mathrm{TX,DN}}$ are denoted as D_R and D_T in Yamada et al. (2022).

Note that there is an upper bound of the return pulse width due to a signal processing characteristic of LIDAR (Yamada et al., 2022). For the return pulse longer than 90 ns (nano second), E_{obs} cannot be calibrated correctly. Therefore, those return pulses were excluded from Equation (23) calculation. Also, there are restrictions on $P_{\mathrm{far,DN}}$ and $P_{\mathrm{TX,DN}}$. $P_{\mathrm{far,DN}}$ less than 11 DU is significantly influenced by the electrical noise, and $P_{\mathrm{far,DN}}$ more than 250 DU is almost saturated. Further, $P_{\mathrm{TX,DN}}$ less than 117 cannot be applied to Equation (25) because of the lack of calibration data. These pulses were disregarded, too. Those unqualified data have been already identified by Yamada et al. (2022) and were excluded from the inputs in advance.

The spacecraft positions are calculated using LIDAR Derived Spacecraft Trajectory SPICE SPK (5.3.2.3.6). We used only data taken at altitudes lower than 9 km by the FAR telescope to ensure the quality of the time series albedo data. We further limited the data to those obtained before a conjunction that started at the end of November 2018 because the FAR telescope was likely contaminated by surface regolith flown by the first touchdown in February 2019. Low and middle-altitude operations were conducted before the conjunction for 15 days (Yamada et al., 2022).

Using Equations (23), (24), and (25), the albedos are calculated preliminarily. However, these preliminary albedos show a cyclic variation. This cycle occurs due to the LIDAR heater ON/OFF switching of about 400-s period (Yamada et al. 2022). To avoid this artifact, we apply bandpass filters to the preliminary albedos. We first combine successive albedos into one segment as long as possible. A series of albedos often includes gaps due to the exclusion of unqualified data described above. If the gap is 20 seconds or less, the missing data within a gap are linearly interpolated. Otherwise, the segments are separated. Next, segments less than 1024 seconds are excluded. This limit is arbitrarily chosen so that the minimum length of the segment is sufficiently longer than the two heater cycles. Then, we apply bandpass filters to remove the frequency components from 0.002 to 0.0032 Hz

(Yamada et al. 2022). Note that this frequency range was written mistakenly by Yamada et al. (2022) and has already been corrected by Yamada et al. (2024). After the bandpass filtering, the albedos within the gaps are removed from the time series albedo data products. The smallest and largest products consist of 4464 and 33056 albedos, respectively.

5.3.2.3.5 LIDAR Derived Albedo Map

This data product is calculated from the LIDAR Derived Time Series Albedo Data (5.3.2.3.4) for 3˚-by-3˚ grids. The item ALBEDO (Table 23) is an average of ρ (Equation (23)) in each grid, and ALBEDO_STDEV (Table 23) is the corrected sample standard deviation. The grids with three or fewer footprints are eliminated following Yamada et al. (2022). LONGITUDE and LATITUDE (Table 23) are the central position of the 3˚-by-3˚ grid.

5.3.2.3.6 LIDAR Derived Spacecraft Trajectory SPICE SPK

Topographic information contained in LIDAR time series data can be used to geometrically correct for the spacecraft position by combining them with a reference shape model. If all information of spacecraft position, LIDAR line-of-sight direction, and observed LIDAR range were perfect, the collective LIDAR footprints would delineate the shape of the asteroid. However, there are various errors affecting the footprint positions, among which the largest is generally the trajectory error, making the resultant LIDAR footprints deviate from the reference shape model. We call this deviation the residual, and search for the best trajectory that minimizes the residual. The following 2-step procedure is employed; (1) by assuming that long-term variation in the residual is due to error in the initial trajectory, we get correction time series in each of X, Y, and Z components by fitting polynomial functions, and (2) we make use of Markov chain Monte Carlo (MCMC) algorithm to explore parameters of additional and fine-tuning correction that further reduce the residuals. We employed SPC model version 20181109 with 3,145,728 facets (ryugu_shape_spc_3m_v20181109.bds; renamed from SHAPE_SPC_3M_v20181109.bds) as the reference shape model. See Matsumoto et al. (2020) for more details.

Matsumoto et al. (2020) describes the routine cases using given HPK (Home Position Keeping) trajectory for which long enough unperturbed arc can be retained. However, there are frequent thrusting during special descent operations, which chop the arc into pieces. As a result, the accuracy of LIDAR-derived trajectory deteriorates because of less topographic information contained in the shorter arc with weaker geometric strength. Errors in directions perpendicular to the LIDAR line-of-sight direction will particularly increase. This situation, however, can be mitigated by employing other initial trajectories that incorporate image data. Such initial trajectories were used for special descending and ascending operations. The initial trajectories obtained by the method described in Yamamoto et al. (2020) were used on 30 September 2019, 1 October 2019, and 13-14 November 2019. For the other special operations, trajectories that are much more accurate than HPK trajectory were used as the input when they are provided by the Hayabusa2 engineering team; one called as OP-NAV trajectory was used on 12-16 September 2019 and 2 October 2019, and one called as ESTM (that means “estimated”) was used for the remaining.

This product is not in the Hayabusa2 LIDAR bundle but in the Hayabusa2 SPICE Kernel Archive bundle.

5.3.3 Data Flow

LIDAR raw, calibrated, and derived data products are built up in sequential data processing steps addressing specific corrections or calibrations. All data products are built from raw telemetry ingested into the SIRIUS database. The LIDAR data processing pipelines query the database directly for new raw science data. The LIDAR data files generated by the pipelines are stored in filesystem prepared

by C-SODA. Figure 4 is a schematic that shows the LIDAR data flow from raw telemetry to derived data products.

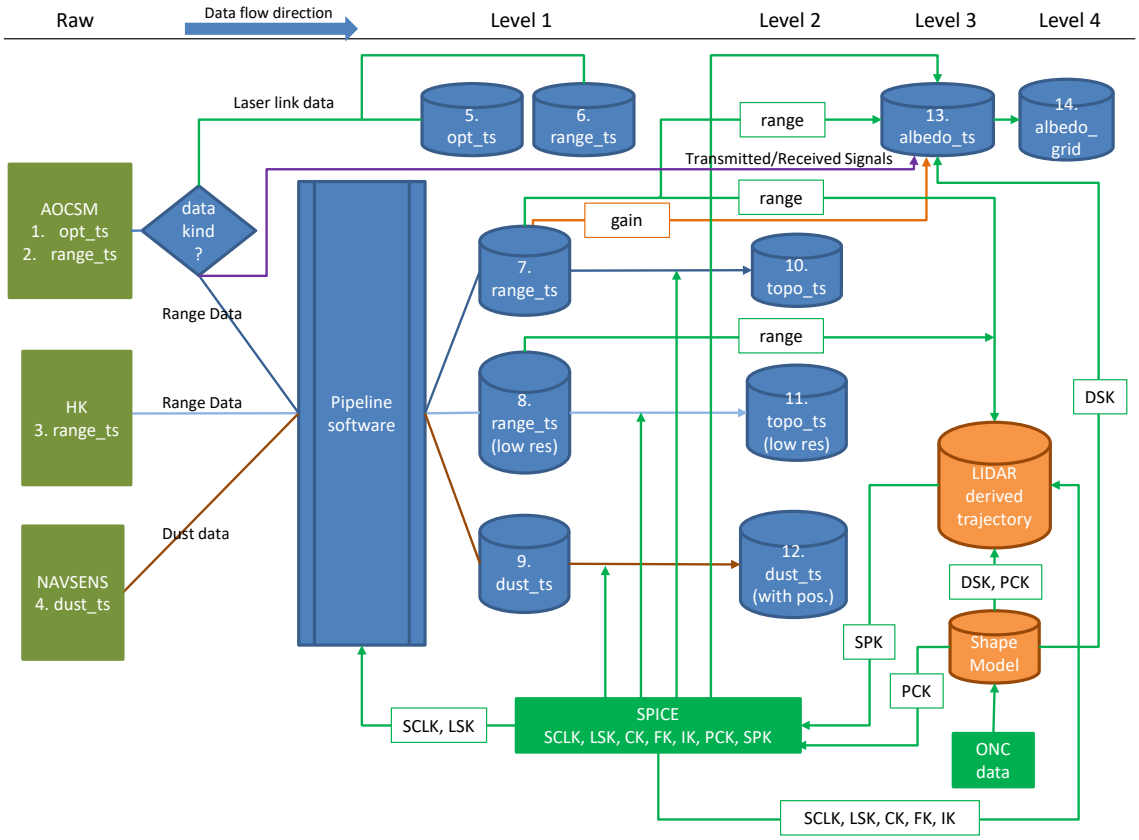

Figure 4. Schematic figure describing data flow.

The observation time in the L1b time series data is converted from TI (Time Indicator) to UTC by using SPICE toolkit, SPICE SCLK, and LSK. The L2 and L3 time series data contain LIDAR footprint position in asteroid-centered body-fixed rotating frame for which a spacecraft trajectory and rotational information are necessary. The rotation parameters are obtained as by-products of shape modeling by Hayabusa2 shape model team. All the L2 and L3 products are based on LIDAR-derived trajectory (see section 5.3.2.3.6). SPICE kernels (SCLK, LSK, CK, FK, IK, and PCK) and LIDAR observation in the L1b data are used as inputs when improving a given initial trajectory (SPK). The L3 albedo time series products are mainly based on energy and range information contained in the L1b time series range data from AOCSM packet, the LIDAR-derived trajectory, and a shape model. The shape model is necessary to simulate returned pulse form. The L4 grid map is created by spatially averaging the L3 time series data.

Table 8 shows the expected LIDAR science data volume by mission phase.

Table 8. LIDAR Data Volume by Mission Phase

Mission phase / Collection directory	Commissioning	EDVEGA	Earth Swing-by	Transfer	Approach	Asteroid Proximity	Return	Reentry
data_raw	0	0	3.8 MiB	0	0	1.1 GiB	1.3 MiB	0
data_link_timing	0	0	406 KiB	0	0	0	0	0
data_intensity	0	0	77 KiB	0	0	0	0	0
data_range	0	0	0	0	0	1.8 GiB	567 KiB	0
data_dust	0	0	0	0	0	58 MiB	0	0
data_albedo	0	0	0	0	0	45 MiB	0	0
data_albedo_map	0	0	0	0	0	<1 MiB	0	0

5.3.4 Labeling and Identification

All LIDAR data products are labeled with PDS4 compliant detached XML labels. These labels describe the content and format of the associated data product. Labels and products are associated by file name with the label having the same name as the data product except that the label file has an .xml extension.

Labels are constructed with the PDS4 Product Class, Product_Observational sub-class. The Product_Observational sub-class describes a set of information objects produced by an observing system. A hierarchical description of the contents of Product_Observational products appears below:

Product_Observational
- Identification_Area – attributes that identify and name an object
  - logical_identifier – a unique identifier
    urn:jaxa:darts:hyb2_lidar:<collection>:<file_name_root>, e.g.,
    urn:jaxa:darts:hyb2_lidar:data_range:hyb2_ldr_l1b_aocsm_range_ts_20180701
  - version_id - version of product
  - title – Short description of product used as the PDS4 search return
  - information_model_version – version of PDS4 information model used to create product
  - product_class – attribute provides the name of the product class (Product_Observational)
- Observation_Area – attributes that provide information about the circumstances under which the data were collected.
  - Time_Coordinates – time attributes of data product
  - Primary_Results_Summary – high-level description of the types of products included in the collection or bundle
  - Investigation_Area – mission, observing campaign or other coordinated, large-scale data collection attributes
  - Observing_System – observing system (instrument) attributes
  - Target_Identification – observation target attributes
  - Discipline_Area – discipline specific attributes needed to describe data product
  - Mission_Area – mission specific attributes needed to describe data product
- File_Area_Observational – describes a file and one or more tagged_data_objects contained within.
  - File – identifies the file that contains one or more data objects
  - Table_Delimited – defines a simple delimited table.

Information in the preceding paragraphs was distilled from the PDS4 Information Model provided by PDS. Additional information on product labels can be found at https://pds.nasa.gov/datastandards/about/.

LIDAR data products except for LIDAR derived spacecraft trajectory SPICE SPK are identified with file names that describe the following elements:

hyb2_ldr_*level*_[*telemetry*_]*product*_[*date*_]*version*.*extension*

where

- level – LIDAR processing level
  - l0, l1b, l2, l3, and l4
- telemetry – type of telemetry, only used for L0, L1b, and L2 time series products
  - aocsm for AOCSM packet
  - hk for HK packet
  - navsens for NAVSENS packet
- product – product type
  - opt_ts for time series laser link timing data
  - laser_link_opt_ts for time series laser link timing data
  - laser_link_range_ts for time series laser link intensity data
  - range_ts for time series range data
  - topo_ts for time series topography data
  - dust_ts for time series dust count data
  - albedo_ts for time series albedo Data
  - albedo_grid for albedo map
- date – date of observation
  - YYYYMMDD where YYYY is year in 4 digits, MM is zero-padded month in 2 digits, and DD is zero-padded day in 2 digits
- version – version of the file
  - v[1]##
  - "1" is added after "v" for range_ts and topo_ts in order to discriminate them from what were internally distributed to the landing site selection team.
- extension – extension of the file

Note that the brackets [] mean the conditional string which is not appeared for some cases, and the variables are written in italic.

Examples of filename are shown below:

1. hyb2_ldr_l0_aocsm_opt_ts_20151211_v01.csv
2. hyb2_ldr_l0_aocsm_range_ts_20180717_v01.csv
3. hyb2_ldr_l0_navsens_dust_ts_20180712_v01.csv
4. hyb2_ldr_l0_hk_range_ts_20190717_v01.csv
5. hyb2_ldr_l1b_aocsm_laser_link_opt_ts_20151211_v01.csv
6. hyb2_ldr_l1b_aocsm_laser_link_range_ts_20151211_v01.csv
7. hyb2_ldr_l1b_aocsm_range_ts_20180717_v101.csv
8. hyb2_ldr_l1b_hk_range_ts_20180717_v101.csv
9. hyb2_ldr_l1b_navsens_dust_ts_20180717_v01.csv

10. hyb2_ldr_l2_aocsm_topo_ts_20180717_v101.csv
11. hyb2_ldr_l2_hk_topo_ts_20180717_v101.csv
12. hyb2_ldr_l2_navsens_dust_ts_20180712_v01.csv
13. hyb2_ldr_l3_albedo_ts_20180720_v01.csv
14. hyb2_ldr_l4_albedo_grid_v01.csv

5.4 Standards Used in Generating Data Products

5.4.1 PDS Standards

All data products described in this SIS conform to PDS4 standards as described in the PDS Standards document noted in the Applicable Documents section of this SIS. Prior to public release, all data products will have passed a PDS peer review to ensure compliance with applicable standards.

In consultation with the PDS, the Hayabusa2 Mission shall use the 1.14.0.0 version of the PDS4 information model. All Hayabusa2 products will conform to this standard, however products may have various versions of specific Discipline Dictionaries.

5.4.2 Time Standards

All Hayabusa2 time series data products contain a UTC time that has been derived from the Hayabusa2 spacecraft clock. The transformation table from the spacecraft clock to UTC is provided by SIRIUS and is converted to SPICE SCLK file by the Hayabusa2 DAC team. This transformation table itself is proprietary; however, the transformation can be achieved by SPICE routines with the SPICE SCLK file included in the Hayabusa2 SPICE Kernel Archive bundle.

5.4.3 Coordinate Systems

All coordinate systems used by the Hayabusa2 mission conform to IAU standards. A complete discussion of the coordinate systems and how they are deployed in the mission can be found in Ryugu Coordinate System Description prepared by the Hayabusa2 Shape Model team, included in document collection of the Hayabusa2 mission bundle.

5.4.4 Data Storage Conventions

All LIDAR data products except for LIDAR derived spacecraft trajectory are stored as ASCII delimiter separated values tables. The standard delimiter of comma has been chosen by the team.

5.5 Data Validation

In addition to software verification and validation, each data product has been peer reviewed for both PDS data format acceptability and scientific usefulness. No changes are expected to data formats after peer review. Should any changes be needed, the configuration control process will be followed and documented.

When data are prepared for submission to the PDS, the DAC team and the LIDAR team will use PDS / mission-provided validation tools for conformance to the PDS4 standards. LIDAR team members and DAC team members will validate the data contained within the LIDAR data products.

6 Detailed Data Product Specifications

The following sections provide detailed data product specifications for each LIDAR data product. These specifications will provide sufficient detail, so that data product users can read and interpret the products.

6.1 Data Product Structure and Organization

The Hayabusa2 data archive is organized by instrument. The LIDAR bundle of the archive is organized by processing level, product type, and mission phase. Data products are stored under each mission phase directory which is just under data collection directory. Which mission phase directory is selected to store data product is determined by value of start_date_time attribute of Product_Observational/Observation_Area/Time_Coordinates class being in which mission phase period. List of collections and products in each collection is summarized in Table 9. These collections are under the Hayabusa2 LIDAR bundle directory, *hyb2_lidar*. Each name of collection is same as directory name in the bundle.

Table 9. List of collections and products in each collection

Directory name of collection	Collection	Products in the collection
data_raw	Hayabusa2 LIDAR Raw Data Collection	● LIDAR Raw Time Series Laser Link Intensity Data ● LIDAR Raw Time Series Laser Link Timing Data ● LIDAR Raw Time Series Dust Count Data ● LIDAR Raw Time Series Range Data ● LIDAR Raw Time Series Low Resolution (HK) Range Data
data_dust	Hayabusa2 LIDAR Calibrated and Derived Dust Count Data Collection	● LIDAR Calibrated Time Series Dust Count Data ● LIDAR Derived Time Series Dust Count Data with Positions
data_link_intensity	Hayabusa2 LIDAR Calibrated Laser Link Experiment Intensity Data Collection	● LIDAR Calibrated Time Series Laser Link Intensity Data
data_link_timing	Hayabusa2 LIDAR Partially Processed Laser Link Experiment Timing Data Collection	● LIDAR Partially Processed Time Series Laser Link Timing Data
data_range	Hayabusa2 LIDAR Calibrated and Derived Range Data Collection	● LIDAR Calibrated Time Series Range Data ● LIDAR Calibrated Time Series Low Resolution (HK) Range Data ● LIDAR Derived Time Series Topography ● LIDAR Derived Time Series Low Resolution (HK) Topography
data_albedo	Hayabusa2 LIDAR Derived Albedo Data Collection	● LIDAR Derived Time Series Albedo Data
data_albedo_map	Hayabusa2 LIDAR Derived Albedo Map Data Collection	● LIDAR Derived Albedo Map
document	Hayabusa2 LIDAR Document Collection	● SIS (This file) and instrument papers

Most of the products are stored as ASCII delimiter separated variable table format with a detached PDS label. The detached PDS labels are PDS4 compliant XML labels that describe the contents of the file. The products are:

1. **LIDAR Raw Time Series Laser Link Timing Data** – These data are a raw time-series of 10-field variable byte records of Laser Link timing. Data are in digital number (DN) format.
2. **LIDAR Raw Time Series Range Data** – These data are a raw time-series of 25-field variable byte records of ranging-related data from AOCSM telemetry. Data are in digital number (DN) format.
3. **LIDAR Raw Time Series Low Resolution (HK) Range Data** – These data are a raw time-series of 8-field variable byte records of ranging-related data from HK telemetry. Data are in digital number (DN) format.
4. **LIDAR Raw Time Series Dust Count Data** – These data are a time-series of 20-field variable byte records of dust-count-related data from NAVSENS telemetry.
5. **LIDAR Partially Processed Time Series Laser Link Timing Data** – These data are a time-series of 5-field variable byte records of Laser Link timing. Only the time when LIDAR starts waiting for laser pulses from a ground station is calibrated.
6. **LIDAR Calibrated Time Series Laser Link Intensity Data** – These data are a time-series of 4-field variable byte records related to transmitting and receiving laser intensities.
7. **LIDAR Calibrated Time Series Range Data** – These data are a time-series of 20-field variable byte records of LIDAR range and intensity data.
8. **LIDAR Calibrated Time Series Low Resolution (HK) Range Data** – These data are a time-series of 6-field variable byte records of LIDAR range and intensity data.
9. **LIDAR Calibrated Time Series Dust Count Data** – These data are a time-series of 7-field variable byte records of threshold, dust detection/non-detection, and wait distance data.
10. **LIDAR Derived Time Series Topography** – These data are a time-series of 11-field variable byte records of LIDAR range from AOCSM, LIDAR footprint position, and spacecraft position data.
11. **LIDAR Derived Time Series Low Resolution (HK) Topography** – These data are a time-series of 11-field variable byte records of LIDAR range from HK, LIDAR footprint position, and spacecraft position data.
12. **LIDAR Derived Time Series Dust Count Data with Positions** – These data are a time-series of 12-field variable byte records of dust detection results, dust count start and end positions, and spacecraft position data.
13. **LIDAR Derived Time Series Albedo Data** – These data are a time-series of 11-field variable byte records of albedo, LIDAR footprint position, and spacecraft position data.
14. **LIDAR Derived Albedo Map** – an albedo map in grid format.

6.2 Data Format Descriptions

In this section, data format is described in detail.

6.2.1 LIDAR Raw Time Series Laser Link Timing Data

The format of the product is described in Table 10. See also the section 5.3.2.1 for the details of the processing.

Table 10. Description of LIDAR Raw Time Series Laser Link Timing Data

	Name	Data Type	Description	Remark
1	PACKET_TIME	ASCII_Time	Packet generation time in UTC. This is just a reference information and is not used to generate L1b data.	Calculated from TI_TIME by SPICE.
2	TI_TIME	ASCII_Numeric_Base16	TI of packet generated time.	
3	DUMP_NUM	ASCII_NonNegative_Integer	A number indicating data position in 16 seconds of data contained in one AOCSM packet.	
4	CMD_TI	ASCII_Numeric_Base16	Lower 2 bytes of TI of command issued time.	
5	LIDAR_MODE	ASCII_NonNegative_Integer	Mode of LIDAR. 0: MEAS (ranging), 1: DUST, 2: OPT (laser link).	
6	VAL_ST	ASCII_NonNegative_Integer	A flag indicating whether status of data transmission from LIDAR to AOCU is valid (1) or invalid (0).	Used for data selection.
7	STOP2_PLS_DET	ASCII_NonNegative_Integer	A flag indicating whether 2nd pulse from ground station is detected (1) or not (0).	Used for data selection.
8	TIMING_STOP1	ASCII_NonNegative_Integer	Count value of interval between first detected pulse from ground station and laser diode trigger time (17 bits).	
9	TIMING_STOP2	ASCII_NonNegative_Integer	Count value of interval between two received pulses from ground laser station.	
10	TIMING_START	ASCII_NonNegative_Integer	Count value of interval between laser diode triggering and laser transmission (17 bits).	

6.2.2 LIDAR Raw Time Series Range Data

The format of the product is described in Table 11. See also the section 5.3.2.1 for the details of the processing.

Table 11. Description of LIDAR Raw Time Series Range Data

	Name	Data Type	Description	Remark
1	PACKET_TIME	ASCII_Time	Packet generation time in UTC. This is just a reference information and is not used to generate L1b data.	Calculated from TI_TIME by SPICE.
2	TI_TIME	ASCII_Numeric_Base16	TI of packet generated time	
3	DUMP_NUM	ASCII_NonNegative_Integer	A number indicating data position in 16 seconds of data contained in one AOCSM packet. The value of 1 and 16 shows the newest and oldest data in the packet, respectively.	
4	CMD_TI	ASCII_Numeric_Base16	Lower 2 bytes of TI of command issued time.	

	Name	Data Type	Description	Remark
5	LIDAR_MODE	ASCII_NonNegative_Integer	Mode of LIDAR. 0: MEAS (ranging), 1: DUST, 2: OPT (laser link)	
6	STOP_OVF	ASCII_NonNegative_Integer	A flag indicating whether counter overflow occurred (1) or not (0) for stop (reception) pulse.	Used for data selection.
7	INTERVAL	ASCII_NonNegative_Integer	Time interval of LIDAR shot command. 1 second (1) or 32 seconds (0).	
8	TX_PLS_DET	ASCII_NonNegative_Integer	A flag indicating whether transmitted pulse detected (1) or not (0).	Used for data selection.
9	RX_PLS_DET_FAR	ASCII_NonNegative_Integer	A flag indicating whether received pulse detected (1) or not (0) for far optics.	Used for data selection.
10	RX_PLS_DET_NEAR	ASCII_NonNegative_Integer	A flag indicating whether received pulse detected (1) or not (0) for near optics.	Used for data selection.
11	VAL_ST	ASCII_NonNegative_Integer	A flag indicating whether status of data transmission from LIDAR to AOCU is valid (1) or invalid (0).	Used for data selection.
12	DN_RX_TELESCOPE	ASCII_NonNegative_Integer	Selected LIDAR optics: far (0) or near (1).	
13	TIMING_RX_FAR	ASCII_NonNegative_Integer	Count value of reception timing for far optics (17bits).	Denoted as $C_{\mathrm{RX,far,DN}}$. Used in Equation (5).
14	TIMING_RX_NEAR	ASCII_NonNegative_Integer	Count value of reception timing for near optics (17bits).	Denoted as $C_{\mathrm{RX,near,DN}}$. Used in Equation (8).
15	TIMING_TX	ASCII_NonNegative_Integer	Count value of interval between laser diode triggering and laser transmission (17 bits).	Denoted as $C_{\mathrm{TX,DN}}$. Equations (5) and (8).
16	DN_INTENS_RX_FAR	ASCII_NonNegative_Integer	Peak value of signal received by far optics.	Denoted as $P_{\mathrm{far,DN}}$. Used in Equations (7) and (13).
17	DN_INTENS_RX_NEAR	ASCII_NonNegative_Integer	Peak value of signal received by near optics.	Denoted as $P_{\mathrm{near,DN}}$. Used in Equations (10) and (14).
18	DN_INTENS_TX	ASCII_NonNegative_Integer	Peak value of transmitted signal.	Denoted as $P_{\mathrm{TX,DN}}$. Used in Equation (11).
19	DN_APD_HV_FAR	ASCII_NonNegative_Integer	APD applied voltage for far range finder.	Contained in sub-word. Used to infer APD_ _FAR in Table 16.

	Name	Data Type	Description	Remark
20	DN_APD_HV_NEAR	ASCII_NonNegative_Integer	APD applied voltage for near range finder.	Contained in sub-word. Used to infer APD_GAIN_NEAR in Table 16.
21	DN_TEMP_RX_APD_FAR	ASCII_NonNegative_Integer	Temperature of APD for far range finder.	Contained in sub-word. Denoted as $T_{\mathrm{APD,far,DN}}$. Used in Equation (15).
22	DN_TEMP_RX_APD_NEAR	ASCII_NonNegative_Integer	Temperature of APD for near range finder.	Contained in sub-word. Denoted as $T_{\mathrm{APD,near,DN}}$. Used in Equation (16).
23	DN_TEMP_RX_PK_FAR	ASCII_NonNegative_Integer	Temperature of peak-detection circuit for far range finder.	Contained in sub-word. Denoted as $T_{\mathrm{RX,far,DN}}$. Used in Equation (17).
24	DN_TEMP_RX_PK_NEAR	ASCII_NonNegative_Integer	Temperature of peak-detection circuit for near range finder.	Contained in sub-word. Denoted as $T_{\mathrm{RX,near,DN}}$. Used in Equation (18).
25	DN_TEMP_TX_PK	ASCII_NonNegative_Integer	Temperature of peak-detection circuit for laser transmitter.	Contained in sub-word. Denoted as $T_{\mathrm{TX,DN}}$. Used in Equation (19).

6.2.3 LIDAR Raw Time Series Low Resolution (HK) Range Data

The format of the product is described in Table 12. See also the section 5.3.2.1 for the details of the processing.

Table 12. Description of LIDAR Raw Time Series Low Resolution (HK) Range Data

	Name	Data Type	Description	Remark
1	PACKET_TIME	ASCII_Time	Packet generation time in UTC. This is just a reference information and is not used to generate L1b data.	Calculated from TI_TIME by SPICE.
2	TI_TIME	ASCII_Numeric_Base16	TI of packet generated time.	
3	LIDAR_MODE	ASCII_NonNegative_Integer	Mode of LIDAR. 0: MEAS (ranging), 1: DUST, 2: OPT (laser link).	
4	DN_RX_TELESCOPE	ASCII_NonNegative_Integer	Selected LIDAR optics: far (0) or near (1).	
5	RANGE	ASCII_NonNegative_Integer	Range data measured by LIDAR that is computed on board. Unit is in m.	Denoted as L_{far} or L_{near} depending on DN_RX_TELESCOPE.

	Name	Data Type	Description	Remark
6	DN_INTENS_RX_FAR	ASCII_NonNegative_Integer	Peak value of signal received by far optics.	Denoted as $P_{\mathrm{far,DN}}$. Used in Equations (7) and (13).
7	DN_INTENS_RX_NEAR	ASCII_NonNegative_Integer	Peak value of signal received by near optics.	Denoted as $P_{\mathrm{near,DN}}$. Used in Equations (10) and (14).
8	DN_TEMP_LD	ASCII_NonNegative_Integer	Temperature of laser diode.	Denoted as $T_{\mathrm{LD,DN}}$. Used in Equation (12).

6.2.4 LIDAR Raw Time Series Dust Count Data

The format of the product is described in Table 13. See also the section 5.3.2.1 for the details of the processing.

Table 13. Description of LIDAR Raw Time Series Dust Count Data

	Name	Data Type	Description	Remark
1	PACKET_TIME	ASCII_Time	Packet generation time in UTC. This is just a reference information and is not used to generate L1b data.	Calculated from TI_TIME by SPICE.
2	TI_TIME	ASCII_Numeric_Base16	TI of packet generated time.	
3	CMD_TI	ASCII_Numeric_Base16	Lower 2 bytes of TI of command issued time.	
4	LIDAR_MODE	ASCII_NonNegative_Integer	Mode of LIDAR. 0: MEAS (ranging), 1: DUST, 2: OPT (laser link).	
5	APD_HV_PWR_FAR	ASCII_NonNegative_Integer	A flag indicating high voltage of APD for far optics is on (1) or off (0).	Used for data selection.
6	RANGE_ENA	ASCII_NonNegative_Integer	A flag indicating ranging is enable (1) or disable (0).	Used for data selection.
7	DUST_COUNT_ENA	ASCII_NonNegative_Integer	A flag indicating dust count is enable (1) or disable (0).	Used for data selection.
8	DN_RX_TELESCOPE	ASCII_NonNegative_Integer	Selected LIDAR optics: far (0) or near (1).	
9	DUST_START_TIMING	ASCII_NonNegative_Integer	Count value of transmission timing (17 bits).	
10	DN_THRESHOLD	ASCII_NonNegative_Integer	Detection threshold for far optics.	See Table 7 to convert to mV.
11	DUST_CNT_01	ASCII_Numeric_Base2	The successive 50 numbers of dust count data. The value of 0 or 1 means non-detection or detection of the laser pulses reflected by dusts (or asteroid surface), respectively. Since the spatial length of the counting range is 1 km which is divided into 50 bins, each bit	

	Name	Data Type	Description	Remark
			corresponds to the bin length of 20 meters in the field-of-view direction. The leftmost and the rightmost bits respectively correspond to the nearest and the farthest points with respect to the spacecraft.	
12	DN_WAIT_DISTANCE	ASCII_NonNegative_Integer	Distance between the spacecraft to the start point of the dust observation in the line-of-sight direction.	Denoted as $D_{\mathrm{wait,DN}}$

6.2.5 LIDAR Partially Processed Time Series Laser Link Timing Data

The format of the product is described in Table 14. The source product is LIDAR Raw Time Series Laser Link Timing Data. See also the section 5.3.2.2.2 for the details of the processing.

Table 14. Description of LIDAR Partially Processed Time Series Laser Link Timing Data

	Name	Data Type	Unit	Description	Remark
1	WAIT_START_TIME	ASCII_Date_Time_YMD_UTC		This value is the time in UTC when a command to start waiting for the laser pulses from a ground station was issued.	Calculated from SCLK_CLOCK_STRING.
2	SCLK_CLOCK_STRING	ASCII_String		This value is SCLK clock string corresponding to WAIT_START_TIME (column 1) that consists of partition number and TI (Time Indicator) with decimal notation. This TI is derived from TI of the packet (TI_TIME), the CMD_TI value for recording timing of issuing command to start waiting for the laser pulses, and the DUMP_NUM value that indicates n-th value in the AOCSM packet.	Equation (1) is used. The TI_TIME, CMD_TI, and DUMP_NUM are found in the source product.
3	TIMING_STOP1	ASCII_NonNegative_Integer		The LIDAR has a 17-bit counter with frequency of approximately 300 MHz (3.3 ns per bit) for ranging. In the laser link mode, the laser diode is triggered by first laser reception, then after a period of laser excitation, shown as TIMING_START, a laser pulse is emitted from the LIDAR. TIMING_STOP1 shows a raw count value of the interval between first detected pulse and laser diode trigger time in this mode.	Copied from TIMING_STOP1 in the source product.
4	TIMING_STOP2	ASCII_NonNegative_Integer		In the laser link mode, the LIDAR can receive up to two laser shots from the ground station during 1-sec waiting period. TIMING_STOP2 shows the interval between two received pulses.	Copied from TIMING_STOP2 in the source product.

	Name	Data Type	Unit	Description	Remark
5	TIMING_START	ASCII_NonNegative_Integer		TIMING_START shows a raw count value of the interval between laser diode trigger time and laser emission after laser diode excitation. Therefore, the internal delay in the instrument is expressed as TIMING_STOP1 + TIMING_START.	Copied from TIMING_START in the source product.

6.2.6 LIDAR Calibrated Time Series Laser Link Intensity Data

The format of the product is described in Table 15. The source product is LIDAR Raw Time Series Dust Count Data. See also the section 5.3.2.2.3 for the details of the processing.

Table 15. Description of LIDAR Calibrate Time Series Laser Link Intensity Data

	Name	Data Type	Unit	Description	Remark
1	SHOT_TIME	ASCII_Date_Time_YMD_UTC		This value is the time in UTC when a command shot the laser was issued.	Calculated from SCLK_CLOCK_STRING and TIMING_TX in the source product.
2	SCLK_CLOCK_STRING	ASCII_String		SCLK clock string corresponding to SHOT_TIME that consists of partition number and TI (Time Indicator) with decimal notation.	Equation (2) is used. The TI_TIME, CMD_TI, and DUMP_NUM are found in the source product.
3	INTENS_RX_FAR	ASCII_Real	mV	The output voltage of APD (Avalanche Photo Diode) of the long-range (FAR) receiving telescope, which is converted from receiving power. The APD gain is set to high (multiplication factor $M = 100$) for these data, and the corresponding responsivity (conversion coefficient from receiving power to output voltage) is 500 kV/W.	Calculated from DN_INTENS_RX_FAR found in the source product using Equation (13).
4	INTENS_TX	ASCII_Real	J	The energy of laser pulse transmitted from the LIDAR in J unit.	Calculated from DN_INTENS_TX found in the source product using Equation (11).

6.2.7 LIDAR Calibrated Time Series Range Data

The format of the product is described in Table 16. The source product is LIDAR Raw Time Series Dust Count Data. See also the section 5.3.2.2.4 for the details of the processing.

Table 16. Description of LIDAR Calibrated Time Series Range Data

	Name	Data Type	Unit	Description	Remark
1	SHOT_TIME	ASCII_Date_Time_YMD_UTC		The UTC time of the laser transmission. It is estimated by using i) upper 2 bytes of spacecraft clock (TI: Time Indicator) of this packet, ii) CMD_TI which is lower 2 bytes of spacecraft clock when the command is issued, and iii) delay time from command to the laser emission.	Calculated from TI_TIME, DUMP_NUM, and CMD_TI using Equations (3) or (4) depending on INTERVAL found in the source product. Further corrected for laser emission delay using TIMING_TX.
2	TI_TIME	ASCII_Numeric_Base16		The spacecraft time called TI (Time Indicator) for this packet, which is the elapsed time since the reset of the counter. One tick of the TI is about 1/32 seconds.	Copied from TI_TIME in the source product.
3	DUMP_NUM	ASCII_NonNegative_Integer		It describes the order of the LIDAR data in the packet. One AOCSM packet contains 16 second LIDAR data. The DUMP_NUM 1 and 16 shows the newest and oldest data in the packet, respectively. In case the laser transmission interval is more than 2 seconds, some of the values in the packet are just copy of previous valid data with "invalid" flag. These invalid data are removed from the product data by using these invalid flags. The time of data with DUMP_NUM is expressed as (DUMP_NUM -1) second before the time converted from TI_TIME.	Copied from DUMP_NUM in the source product.
4	CMD_TI	ASCII_Numeric_Base16		The lower 2 bytes of the spacecraft time (TI: Time Indicator) which corresponds to the time when a command is issued from AOCU to LIDAR. One tick of the TI is about 1/32 seconds. The command from AOCU reaches to LIDAR after about 3 ticks of TI, with uncertainty of ±1 tick of TI.	Copied from CMD_TI in the source product.
5	RX_TELESCOPE	ASCII_String		The kind of receiving telescope and range finder circuit system which is selected by user command. Two types of system are available, long-range (FAR) and short-range (NEAR). The two systems are switched over at a distance between spacecraft and asteroid of about 300 m.	Directly converted from DN_RX_TELESCOPE in the source product.
6	RANGE_FAR	ASCII_Real	m	The distance between spacecraft and asteroid surface measured by long-range	L_{far} in Equation (5). Calculated from

	Name	Data Type	Unit	Description	Remark
				(FAR) telescope system, which is calculated from the count values of laser emission and reception. The resolution is 0.5 m. The internal delay time in the LIDAR is taken into account. If RX_PLS_DET_FAR is 0 in the source product, RANGE_FAR is set to -99999.	TIMING_RX_FAR ($C_{RX,far,DN}$), TIMING_TX ($C_{TX,DN}$), and DN_INTENS_RX_FAR ($P_{far,DN}$) in the source product.
7	RANGE_NEAR	ASCII_Real	m	The distance between spacecraft and asteroid surface measured by short-range (NEAR) telescope system, which is calculated from the count values of laser emission and reception. The resolution is 0.5 m. The internal delay time in the LIDAR is taken into account. If RX_PLS_DET_NEAR is 0 in the source product, RANGE_NEAR is set to -99999.	L_{near} in Equation (8). Calculated from TIMING_RX_NEAR ($C_{RX,near,DN}$), TIMING_TX ($C_{TX,DN}$), and DN_INTENS_RX_NEAR ($P_{near,DN}$) in the source product
8	TIMING_RX_FAR	ASCII_NonNegative_Integer		The value of range finder counter when the return laser pulse is detected by the long-range (FAR) system. The counter resolution is about 3.33 ns (300 MHz), which corresponds to 0.5 m as 1-way range. The value is invalid if the long-range (FAR) system is not used.	$C_{RX,far,DN}$ in Equation (5). Copied from TIMING_RX_FAR in the source product.
9	TIMING_RX_NEAR	ASCII_NonNegative_Integer		The value of range finder counter when the return laser pulse is detected by the short-range (NEAR) system. The counter resolution is about 3.33 ns (300 MHz), which corresponds to 0.5 m as 1-way range. The value is invalid if the short-range (NEAR) system is not used.	$C_{RX,near,DN}$ in Equation (8). Copied from TIMING_RX_NEAR in the source product.
10	TIMING_TX	ASCII_NonNegative_Integer		The elapsed value of range finder counters between the trigger of the laser diode and start pulse detection (i.e., the start of the laser transmission). The counter resolution is about 3.33 ns (300 MHz), which corresponds to 0.5 m as 1-way range.	$C_{TX,DN}$ in Equations (5) and (8). Copied from TIMING_TX in the source product.
11	INTENS_RX_FAR	ASCII_Real	mV	The peak value of laser power received by the APD (Avalanche Photo Diode) for long-range (FAR) system in mV (milli Volt) unit. The peak value can be converted to laser power in W (Watt) unit by using responsivity (conversion coefficient from receiving power to output voltage). The responsivity depends on the value of APD_GAIN_FAR (1, 2, 4, 8) and corresponding multiplication factor M (0.1, 10, 33, 100). The responsivity values for APD_GAIN_FAR = 2, 4, and 8 are about	$I_{RX,far}$ in Equation (13). Calculated from DN_INTENS_RX_FAR ($P_{far,DN}$) in the source product using Equation (13).

	Name	Data Type	Unit	Description	Remark
				50 kV/W, 165 kV/W, and 500 kV/W, respectively (Yamada et al., 2017).	
12	INTENS_RX_NEAR	ASCII_Real	mV	The peak value of laser power received by the APD (Avalanche Photo Diode) for short-range (NEAR) system in mV (milli Volt) unit. APD_GAIN_NEAR of 1, 2, 4, and 8 correspond to multiplication factor M of 0.1, 10, 33, and 100, respectively. The responsivity for NEAR optics is not calibrated.	$I_{RX,near}$ in Equation (14). Calculated from DN_INTENS_RX_NEAR ($P_{near,DN}$) in the source product using Equation (14).
13	INTENS_TX	ASCII_Real	J	The energy of transmitted laser pulse which is estimated from the output of the Pin Photo Diode which detects parts of the laser. The unit is J.	I_{TX} in Equation (11). Calculated from DN_INTENS_TX ($P_{TX,DN}$) and DN_TEMP_LD ($T_{LD,DN}$) in HK.
14	APD_GAIN_FAR	ASCII_Integer		Integer number indicating parameter for APD gain (1, 2, 4 or 8) of the long-range (FAR) range finder circuit. If DN_APD_HV_FAR ≤ 1000 in the source product, this value is set to -99999.	Determined by the table using DN_APD_HV_FAR in the section 5.3.2.2.4.
15	APD_GAIN_NEAR	ASCII_Integer		Integer number indicating parameter for APD gain (1, 2, 4 or 8) of the short-range (NEAR) range finder circuit. If DN_APD_HV_NEAR ≤ 1000 in the source product, this value is set to -99999.	Determined by the table using DN_APD_HV_NEAR in the section 5.3.2.2.4.
16	TEMP_RX_APD_FAR	ASCII_Real	degC	The temperature of APD (Avalanche Photo Diode) in the long-range (FAR) range finder circuit. If the calculated value is less than -10 degC or greater than 45 degC, -99999 is set as invalid constant.	$T_{RX,APD,far}$ in Equation (15). Calculated from DN_TEMP_RX_APD_FAR ($T_{APD,far,DN}$) using Equation (15).
17	TEMP_RX_APD_NEAR	ASCII_Real	degC	The temperature of APD (Avalanche Photo Diode) in the short-range (NEAR) range finder circuit. If the calculated value is less than -10 degC or greater than 45 degC, -99999 is set as invalid constant.	$T_{APD,near,DN}$ in Equation (16). Calculated from DN_TEMP_RX_APD_NEAR using Equation (16).
18	TEMP_RX_PK_FAR	ASCII_Real	degC	The temperature of the peak-detection circuit in the long-range (FAR) range finder circuit. If the calculated value is less than -10 degC or greater than 70 degC, -99999 is set as invalid constant.	$T_{RX,far,DN}$ in Equation (17). Calculated from DN_TEMP_RX_PK_FAR using Equation (17).
19	TEMP_RX_PK_NEAR	ASCII_Real	degC	The temperature of the peak-detection circuit in the short-range (NEAR) range	$T_{RX,near,DN}$ in Equation (18).

	Name	Data Type	Unit	Description	Remark
				finder circuit. If the calculated value is less than -10 degC or greater than 70 degC, -99999 is set as invalid constant.	Calculated from DN_TEMP_RX_PK_NEAR using Equation (18).
20	TEMP_TX_PK	ASCII_Real	degC	The temperature of the peak-detection circuit in the laser transmitter. If the calculated value is less than -10 degC or greater than 70 degC, -99999 is set as invalid constant.	$T_{TX,DN}$ in Equation (19). Calculated from DN_TEMP_TX_PK using Equation (19).

6.2.8 LIDAR Calibrated Time Series Low Resolution (HK) Range Data

The format of the product is described in Table 17. The source product is LIDAR Raw Time Series Low Resolution (HK) Range Data. See also the section 5.3.2.2.5 for the details of the processing.

Table 17. Description of LIDAR Calibrated Time Series Low Resolution (HK) Range Data

	Name	Data Type	Unit	Description	Remark
1	SHOT_TIME	ASCII_Date_Time_YMD_UTC		The UTC time of the laser transmission.	Calculated from TI_TIME, DUMP_NUM, CMD_TI using Equation (3) or (4) depending on INTERVAL. Further corrected for laser emission delay using TIMING_TX. TI_TIME is found in the source product, and the others are found in the AOCSM packet.
2	TI_TIME	ASCII_Numeric_Base16		The spacecraft time called TI (Time Indicator) for this packet, which is the elapsed time since the reset of the counter. One tick of the TI is about 1/32 seconds.	Copied from TI_TIME in the source product.
3	RX_TELESCOPE	ASCII_String		The kind of receiving telescope and range finder circuit system which is selected by user command. Two types of system are available, long-range (FAR) and short-range (NEAR). The two systems are switched over at a distance between spacecraft and asteroid of about 300 m.	Directly converted from DN_RX_TELESCOPE in the source product.
4	RANGE	ASCII_Real	m	The measured distance between the spacecraft and the asteroid surface by long-range (FAR) or short-range (NEAR) telescope system in meter unit.	Copied from RANGE in the source product.

	Name	Data Type	Unit	Description	Remark
				The resolution is 1 m. The internal delay time in the LIDAR is taken into account.	
5	INTENS_RX_FAR	ASCII_Real	mV	The peak value of laser power received by the APD (Avalanche Photo Diode) for long-range (FAR) system in mV (milli Volt) unit. The peak value can be converted to laser power in W (Watt) unit by using responsivity (conversion coefficient from receiving power to output voltage). The responsivity depends on the value of APD_GAIN_FAR (1, 2, 4, 8) and corresponding multiplication factor M (0.1, 10, 33, 100). The responsivity values for APD_GAIN_FAR = 2, 4, and 8 are about 50 kV/W, 165 kV/W, and 500 kV/W, respectively (Yamada et al., 2017).	$I_{RX,far}$ in Equation (13). Calculated from DN_INTENS_RX_FAR in the source product using Equation (13).
6	INTENS_RX_NEAR	ASCII_Real	mV	The peak value of laser power received by the APD (Avalanche Photo Diode) for short-range (NEAR) system in mV (milli Volt) unit. APD_GAIN_NEAR of 1, 2, 4, and 8 correspond to multiplication factor M of 0.1, 10, 33, and 100, respectively. The responsivity for NEAR optics is not calibrated.	$I_{RX,near}$ in Equation (14). Calculated from DN_INTENS_RX_NEAR in the source product using Equation (14).

6.2.9 LIDAR Calibrated Time Series Dust Count Data

The format of the product is described in Table 18. The source product is LIDAR Raw Time Series Dust Count Data. See also the section 5.3.2.2.6 for the details of the processing.

Table 18. Description of LIDAR Calibrated Time Series Dust Count Data

	Name	Data Type	Unit	Description	Remark
1	SHOT_TIME	ASCII_Date_Time_YMD_UTC		The UTC time of the laser transmission. It is estimated by using i) upper 2 bytes of spacecraft clock (TI: Time Indicator) of this packet, ii) CMD_TI which is lower 2 bytes of spacecraft clock when the command is issued, and iii) delay time from command to the laser emission.	Calculated from TI_TIME and CMD_TI using Equation (4). Further corrected for laser emission delay using DUST_START_TIMING.
2	TI_TIME	ASCII_Numeric_Base16		The spacecraft time called TI (Time Indicator) for this packet, which is the elapsed time since the reset of the counter. One tick of the TI is about 1/32 seconds.	Copied from TI_TIME in the source product.
3	CMD_TI	ASCII_Numeric_Base16		The lower 2 bytes of the spacecraft time (TI: Time Indicator) which corresponds to the time when a command is issued	Copied from CMD_TI in the source product.

	Name	Data Type	Unit	Description	Remark
				from AOCU to LIDAR. One tick of the TI is about 1/32 seconds. The command from AOCU reaches to LIDAR after about 3 ticks of TI, with uncertainty of ±1 tick of TI.	
4	DUST_START_TIMING	ASCII_NonNegative_Integer		The elapsed value of range finder counters between laser diode triggering and start pulse detection (i.e., the start of the laser transmission). The counter resolution is about 3.33 ns (300 MHz), which corresponds to 0.5 m as 1-way range.	Copied from DUST_START_TIMING in the source product.
5	THRESHOLD	ASCII_Real	mV	The detection threshold of the laser reception level for long-range (FAR) range finder circuit. The threshold is specified by a user command. The unit is mV (milli Volt). The APD gain is set to high (multiplication factor $M = 100$) for the dust count mode. By using the corresponding responsivity of the APD for high gain (500 kV/W), the threshold level (in mV) can be converted to reception power in W unit.	Calculated from DN_THRESHOLD in the source product using Table 7.
6	DUST_CNT_01	ASCII_Numeric_Base2		The successive 50 numbers of dust count data. The value of 0 or 1 means non-detection or detection of the laser pulses reflected by dusts (or asteroid surface), respectively. Since the spatial length of the counting range is 1 km which is divided into 50 bins, each bit corresponds to the bin length of 20 meters in the line-of-sight direction. The leftmost and the rightmost bits respectively correspond to the nearest and the farthest points with respect to the spacecraft.	Copied from DUST_CNT_01 in the source product.
7	WAIT_DISTANCE	ASCII_NonNegative_Integer	m	The distance between the spacecraft to the start point of the dust observation in the line-of-sight direction in meter unit.	Calculated from DN_WAIT_DISTANCE in the source product using Equation (20).

6.2.10 LIDAR Derived Time Series Topography

The format of the product is described in Table 19. The source product is LIDAR Calibrated Time Series Range Data. See also the section 5.3.2.3.1 for the details of the processing.

Table 19. Description of LIDAR Derived Time Series Topography

	Name	Data Type	Unit	Description	Remark
1	SHOT_TIME	ASCII_Date_Time_YMD_UTC		The UTC time of the laser transmission.	Copied SHOT_TIME in the source product.
2	RANGE	ASCII_Real	m	The distance between spacecraft and asteroid surface calculated from the count values of laser emission and reception. The resolution is 0.5 m. The internal delay time in the LIDAR is taken into account.	Copied RANGE_FAR or RANGE_NEAR depending on the value of RX_TELESCOPE in the source product.
3	TOPO_LONGITUDE	ASCII_Real	deg	The longitude of a laser footprint center position in the asteroid-fixed coordinates, converted from the inertial coordinates by using asteroid ephemeris, and axis and phase of the asteroid rotation.	Calculated by the SPICE using SHOT_TIME, RANGE, and Equation (21).
4	TOPO_LATITUDE	ASCII_Real	deg	The latitude of a laser footprint center position in the asteroid-fixed coordinates, converted from the inertial coordinates by using asteroid ephemeris, and axis and phase of the asteroid rotation.	Same as the above.
5	TOPO_HEIGHT	ASCII_Real	m	The height of a laser footprint center position with respect to the center of the asteroid in the asteroid-fixed coordinates, converted from the inertial coordinates by using asteroid ephemeris, and axis and phase of the asteroid rotation.	Same as the above.
6	TOPO_X	ASCII_Real	m	The X component of a laser footprint center position in the asteroid-fixed coordinates, converted from the inertial coordinates by using asteroid ephemeris, and axis and phase of the asteroid rotation.	Same as the above.
7	TOPO_Y	ASCII_Real	m	The Y component of a laser footprint center position in the asteroid-fixed coordinates, converted from the inertial coordinates by using asteroid ephemeris, and axis and phase of the asteroid rotation.	Same as the above.
8	TOPO_Z	ASCII_Real	m	The Z component of a laser footprint center position in the asteroid-fixed coordinates, converted from the inertial coordinates by using asteroid ephemeris, and axis and phase of the asteroid rotation.	Same as the above.
9	SC_POS_X	ASCII_Real	m	The X component of the spacecraft position in the asteroid-fixed coordinates, converted from the inertial	Calculated by the SPICE at the time of SHOT_TIME.

	Name	Data Type	Unit	Description	Remark
				coordinates by using asteroid ephemeris, and axis and phase of the asteroid rotation.	
10	SC_POS_Y	ASCII_Real	m	The Y component of the spacecraft position in the asteroid-fixed coordinates, converted from the inertial coordinates by using asteroid ephemeris, and axis and phase of the asteroid rotation.	Same as the above.
11	SC_POS_Z	ASCII_Real	m	The Z component of the spacecraft position in the asteroid-fixed coordinates, converted from the inertial coordinates by using asteroid ephemeris, and axis and phase of the asteroid rotation.	Same as the above.

6.2.11 LIDAR Derived Time Series Low Resolution (HK) Topography

The format of the product is described in Table 20. The source product is LIDAR Calibrated Time Series Low Resolution (HK) Range Data. See also the section 5.3.2.3.2 for the details of the processing.

Table 20. Description of LIDAR Derived Time Series Low Resolution (HK) Topography

	Name	Data Type	Unit	Description	Remark
1	SHOT_TIME	ASCII_Date_Time_YMD_UTC		The UTC time of the laser transmission.	Copied from SHOT_TIME in the source product.
2	RANGE	ASCII_Real	m	The distance between spacecraft and asteroid surface calculated from the count values of laser emission and reception. The resolution is 1 m. The internal delay time in the LIDAR is taken into account.	Copied from RANGE_FAR or RANGE_NEAR depending on the value of RX_TELESCOPE in the source product.
3	TOPO_LONGITUDE	ASCII_Real	deg	The longitude of a laser footprint center position in the asteroid-fixed coordinates, converted from the inertial coordinates by using asteroid ephemeris, and axis and phase of the asteroid rotation.	Calculated by the SPICE using SHOT_TIME, RANGE, and Equation (21).
4	TOPO_LATITUDE	ASCII_Real	deg	The latitude of a laser footprint center position in the asteroid-fixed coordinates, converted from the inertial coordinates by using asteroid ephemeris, and axis and phase of the asteroid rotation.	Same as the above.
5	TOPO_HEIGHT	ASCII_Real	m	The height of a laser footprint center position with respect to the center of the asteroid in the asteroid-fixed coordinates, converted from the inertial coordinates by using asteroid	Same as the above.

	Name	Data Type	Unit	Description	Remark
				ephemeris, and axis and phase of the asteroid rotation.	
6	TOPO_X	ASCII_Real	m	The X component of a laser footprint center position in the asteroid-fixed coordinates, converted from the inertial coordinates by using asteroid ephemeris, and axis and phase of the asteroid rotation.	Same as the above.
7	TOPO_Y	ASCII_Real	m	The Y component of a laser footprint center position in the asteroid-fixed coordinates, converted from the inertial coordinates by using asteroid ephemeris, and axis and phase of the asteroid rotation.	Same as the above.
8	TOPO_Z	ASCII_Real	m	The Z component of a laser footprint center position in the asteroid-fixed coordinates, converted from the inertial coordinates by using asteroid ephemeris, and axis and phase of the asteroid rotation.	Same as the above.
9	SC_POS_X	ASCII_Real	m	The X component of the spacecraft position in the asteroid-fixed coordinates, converted from the inertial coordinates by using asteroid ephemeris, and axis and phase of the asteroid rotation.	Calculated by the SPICE at the time of SHOT_TIME.
10	SC_POS_Y	ASCII_Real	m	The Y component of the spacecraft position in the asteroid-fixed coordinates, converted from the inertial coordinates by using asteroid ephemeris, and axis and phase of the asteroid rotation.	Same as the above.
11	SC_POS_Z	ASCII_Real	m	The Z component of the spacecraft position in the asteroid-fixed coordinates, converted from the inertial coordinates by using asteroid ephemeris, and axis and phase of the asteroid rotation.	Same as the above.

6.2.12 LIDAR Derived Time Series Dust Count Data with Positions

The format of the product is described in Table 21. The source product is LIDAR Calibrated Time Series Dust Count Data. See also the section 5.3.2.3.3 for the details of the processing.

Table 21. Description of LIDAR Derived Time Series Dust Count Data with Positions

	Name	Data Type	Unit	Description	Remark
1	SHOT_TIME	ASCII_Date_Time_YMD_UTC		The UTC time of the laser transmission.	Copied SHOT_TIME in the source product.

	Name	Data Type	Unit	Description	Remark
2	THRESHOLD	ASCII_Real	mV	The detection threshold of the laser reception level for long-range (FAR) range finder circuit. The threshold is specified by a user command. The unit is mV (milli Volt). The APD gain is set to high (multiplication factor M = 100) for the dust count mode. By using the corresponding responsivity of the APD for high gain (500 kV/W), the threshold level (in mV) can be converted to reception power in W unit.	Copied THRESHOLD in the source product.
3	DUST_CNT_01	ASCII_Numeric_Base2		The successive 50 numbers of dust count data. The value of 0 or 1 means non-detection or detection of the laser pulses reflected by dusts (or asteroid surface), respectively. Since the spatial length of the counting range is 1 km which is divided into 50 bins, each bit corresponds to the bin length of 20 meters in the line-of-sight direction. The leftmost and the rightmost bits respectively correspond to the nearest and the farthest points with respect to the spacecraft.	Copied DUST_CNT_01 in the source product.
4	DUST_START_X	ASCII_Real	m	The X component of the dust count starting position in the asteroid-fixed coordinates, converted from the inertial coordinates by using asteroid ephemeris, and axis and phase of the asteroid rotation.	Calculated from SHOT_TIME using SPICE by replacing R with D_{wait} in Equation (21).
5	DUST_START_Y	ASCII_Real	m	The Y component of the dust count starting position in the asteroid-fixed coordinates, converted from the inertial coordinates by using asteroid ephemeris, and axis and phase of the asteroid rotation.	Same as the above.
6	DUST_START_Z	ASCII_Real	m	The Z component of the dust count starting position in the asteroid-fixed coordinates, converted from the inertial coordinates by using asteroid ephemeris, and axis and phase of the asteroid rotation.	Same as the above.
7	DUST_END_X	ASCII_Real	m	The X component of the dust count ending position in the asteroid-fixed coordinates, converted from the inertial coordinates by using asteroid ephemeris, and axis and phase of the asteroid rotation.	Calculated from SHOT_TIME using SPICE by replacing R with $D_{\text{wait}} + 1000$ m in Equation (21).

	Name	Data Type	Unit	Description	Remark
8	DUST_END_Y	ASCII_Real	m	The Y component of the dust count ending position in the asteroid-fixed coordinates, converted from the inertial coordinates by using asteroid ephemeris, and axis and phase of the asteroid rotation.	Same as the above.
9	DUST_END_Z	ASCII_Real	m	The Z component of the dust count ending position in the asteroid-fixed coordinates, converted from the inertial coordinates by using asteroid ephemeris, and axis and phase of the asteroid rotation.	Same as the above.
10	SC_POS_X	ASCII_Real	m	The X component of the spacecraft position in the asteroid-fixed coordinates, converted from the inertial coordinates by using asteroid ephemeris, and axis and phase of the asteroid rotation.	Calculated from SHOT_TIME using SPICE.
11	SC_POS_Y	ASCII_Real	m	The Y component of the spacecraft position in the asteroid-fixed coordinates, converted from the inertial coordinates by using asteroid ephemeris, and axis and phase of the asteroid rotation.	Same as the above.
12	SC_POS_Z	ASCII_Real	m	The Z component of the spacecraft position in the asteroid-fixed coordinates, converted from the inertial coordinates by using asteroid ephemeris, and axis and phase of the asteroid rotation.	Same as the above.

6.2.13 LIDAR Derived Time Series Albedo Data

The format of the product is described in Table 22. The source products are LIDAR Raw Time Series Range Data, LIDAR Calibrated Time Series Range Data, and LIDAR Calibrated Time Series Range Low Resolution (HK) Data. See also the section 5.3.2.3.4 for the details of the processing.

Table 22. Description of LIDAR Derived Time Series Albedo Data

	Name	Data Type	Unit	Description	Remark
1	SHOT_TIME	ASCII_Date_Time_YMD_UTC		The UTC time of the laser transmission.	Copied SHOT_TIME in the source product.
2	ALBEDO	ASCII_Real		The albedo value estimated at the footprint position.	ρ in Equation (23). Calculated from DN_INTENS_RX_FAR, DN_INTENS_TX, GAIN, and RANGE_FAR using Equations (23), (24), and (25). Further corrected for a cyclic

	Name	Data Type	Unit	Description	Remark
					variation by removing the frequency components from 0.002 to 0.0032 Hz.
3	TOPO_LONGITUDE	ASCII_Real	deg	The longitude of a laser footprint center position in the asteroid-fixed coordinates, converted from the inertial coordinates by using asteroid ephemeris, and axis and phase of the asteroid rotation.	Calculated by the SPICE using SHOT_TIME, RANGE in the source product, and Equation (21).
4	TOPO_LATITUDE	ASCII_Real	deg	The latitude of a laser footprint center position in the asteroid-fixed coordinates, converted from the inertial coordinates by using asteroid ephemeris, and axis and phase of the asteroid rotation.	Same as the above.
5	TOPO_HEIGHT	ASCII_Real	m	The height of a laser footprint center position with respect to the center of the asteroid in the asteroid-fixed coordinates, converted from the inertial coordinates by using asteroid ephemeris, and axis and phase of the asteroid rotation.	Same as the above.
6	TOPO_X	ASCII_Real	m	The X component of a laser footprint center position in the asteroid-fixed coordinates, converted from the inertial coordinates by using asteroid ephemeris, and axis and phase of the asteroid rotation.	Same as the above.
7	TOPO_Y	ASCII_Real	m	The Y component of a laser footprint center position in the asteroid-fixed coordinates, converted from the inertial coordinates by using asteroid ephemeris, and axis and phase of the asteroid rotation.	Same as the above.
8	TOPO_Z	ASCII_Real	m	The Z component of a laser footprint center position in the asteroid-fixed coordinates, converted from the inertial coordinates by using asteroid ephemeris, and axis and phase of the asteroid rotation.	Same as the above.
9	SC_POS_X	ASCII_Real	m	The X component of the spacecraft position in the asteroid-fixed coordinates, converted from the inertial coordinates by using asteroid ephemeris, and axis and phase of the asteroid rotation.	Calculated using the LIDAR Derived Spacecraft Trajectory SPICE SPK (5.3.2.3.6).
10	SC_POS_Y	ASCII_Real	m	The Y component of the spacecraft position in the asteroid-fixed coordinates, converted from the inertial coordinates by using asteroid	Same as the above.

	Name	Data Type	Unit	Description	Remark
				ephemeris, and axis and phase of the asteroid rotation.	
11	SC_POS_Z	ASCII_Real	m	The Z component of the spacecraft position in the asteroid-fixed coordinates, converted from the inertial coordinates by using asteroid ephemeris, and axis and phase of the asteroid rotation.	Same as the above.

6.2.14 LIDAR Derived Albedo Map

The format of the product is described in Table 23. The gridded albedo is calculated by averaging the albedo values whose expected footprint center are included in the grid. The map is in pixel registration. The source product is LIDAR Derived Time Series Albedo Data. See also the section 5.3.2.3.5 for the details of the processing.

Table 23. Description of LIDAR Derived Albedo Map

	Name	Data Type	Unit	Description	Remark
1	LONGITUDE	ASCII_Real	deg	The center longitude of the 3˚-by-3˚ grid.	
2	LATITUDE	ASCII_Real	deg	The center latitude of the 3˚-by-3˚ grid.	
3	ALBEDO_AVE	ASCII_Real		The average albedo within the 3˚-by-3˚ grid.	Calculated from ALBEDO in the source product.
4	ALBEDO_STDEV	ASCII_Real		The corrected sample standard deviation of the albedo within the 3˚-by-3˚ grid.	Same as above.

7 Applicable Software

7.1 Utility Programs

At the current time, the Hayabusa2 project has no plans to release any mission specific utility programs.

7.2 Applicable PDS Software Tools

Data products found in the Hayabusa2 archive can be viewed with any PDS4 compatible software utility. A listing of these tools can be found at https://pds.nasa.gov/tools/about/ .

7.3 Software Distribution and Update Procedures

As no Hayabusa2 specific software will be released to the public, this section is not applicable.

8 Appendices

8.1 Definitions of Data Processing Levels

PDS4 Data Processing Levels (From PDS Policy on Data Processing Levels (2013-03-11):

Telemetry: An encoded byte stream used to transfer data from one or more instruments to temporary storage where the raw instrument data will be extracted.

Raw: Original data from an instrument. If compression, reformatting, packetization, or other translation has been applied to facilitate data transmission or storage, those processes will be reversed so that the archived data are in a PDS approved archive format.

Partially Processed: Data that have been processed beyond the raw stage but which have not yet reached calibrated status.

Calibrated: Data converted to physical units, which makes values independent of the instrument.

Derived: Results that have been distilled from one or more calibrated data products (for example, maps, gravity or magnetic fields, or ring particle size distributions). Supplementary data, such as calibration tables or tables of viewing geometry, used to interpret observational data should also be classified as ‘derived’ data if not easily matched to one of the other three categories.